Journal of Sedimentary Research
Article In Press
Acceptation date : July 2024
https://doi.org/10.2110/jsr.2024.024
https://archimer.ifremer.fr/doc/00901/101308/

Anatomy of Niger and Benue river sediments from clay to granule: grain-size dependence and provenance budgets

Garzanti Eduardo [1,*], Bayon Germain [2], Barbarano Marta [1], Resentini Alberto [1], Vezzoli Giovanni [1], Pastore Guido [1], Levacher Mathilde [2], Adeaga Olusegun [3]

[1] Laboratory for Provenance Studies, Department of Earth and Environmental Sciences, University of Milano-Bicocca, 20126 Milano, Italy
[2] Unité de Recherche Geosciences Marines, Ifremer, CS 10070, 29280 Plouzané, France
[3] Department of Geography, University of Lagos, Yaba, Lagos, Nigeria

* Corresponding author : Eduardo Garzanti, email address : eduardo.garzanti@unimib.it

Abstract :

This study explores in detail the complexity of textural/compositional relationships in fluvial sediments. To this aim, fifteen size fractions (from clay to granule) of three sediment samples characterized by virtually identical size distribution from the Niger and Benue rivers in central Nigeria were separately analysed by multiple methods (optical microscopy, manual and semi-automated Raman spectroscopy, X-ray diffraction, elemental geochemistry, Nd isotopes). The independent mineralogical and geochemical datasets thus obtained allowed us to investigate processes of sediment generation for five diverse size modes (clay, fine cohesive silt, very coarse frictional silt, very fine sand, coarse sand) derived in different proportions from different sources (wind-blown dust, soils and paleosols, fine-grained and coarse-grained siliciclastic units, igneous and metamorphic bedrocks). Controls on the size distribution of detrital minerals (settling equivalence, size inheritance, weathering, mechanical durabil ity, and chemical durability through multiple sedimentary cycles) were examined, specifically focusing on tectosilicates and on the long-standing petrological problem of feldspar-grain size relations. Different factors determine the composition of different size modes: kaolinite-dominated clay derives from both deeply weathered soils or paleosols and distant Saharan sources; cohesive silt is largely recycled from soils formed in sedimentary basins. The proportion of detritus derived first-cycle from basement rocks increases from very coarse silt to very fine sand, whereas the coarse sand mode is quartz-dominated with minor plagioclase and amphibole and local occurrence of garnet, staurolite, monazite, or xenotime reflecting a combined influence of size inheritance from igneous (pegmatite) and metamorphic sources, mechanical and chemical durability, and recycling from coarse-grained siliciclastic units. Sediment budgets based on mineralogical, geochemical, and geochronological signatures consistently indicate dominance of Benue sediment supply, although contributions from the Niger mainstem to the Niger Delta are inferred to have been notably greater in the wetter past, before clastic fluxes dropped in response to the aridification of the Sahel.

Keywords : Intrasample mineralogical and geochemical variability, Quartz/feldspar ratio, REE, Zr/Hf, and Nd isotopes, Processes of clay, silt, and sand generation, Sediment yields and erosion rates, Niger and Benue rivers, Nigeria

INTRODUCTION

The composition of siliciclastic sediments is markedly influenced by various controls operating during pedogenesis, erosion, transport and deposition, which combine in a complicated web of links and feedbacks (Johnsson 1993). Exploring the multifaceted nature of textural/compositional relationships represents a fundamental pre-requisite to unravel the complex processes of sediment generation.

Grain size is the principal textural property of sediments and sedimentary rocks (e.g., Folk 1980; Ibbeken and Schleyer 1991). In siliciclastic sediment, every compositional parameter is grain-size dependent (Whitmore et al. 2004; von Eynatten et al. 2012, 2016). Grain-size dependence is controlled in turn by several interplaying factors, including texture and mineralogy of source rocks, comminution by a combination of physical (i.e., mechanical abrasion and breakage) and chemical processes (i.e., dissolution and replacement), and hydraulic sorting during transport, deposition, and reworking by tractive currents.

This study is part of a larger project on the entire Niger River sediment-routing system from Guinea to the ocean, and companion to papers focusing specifically on detrital-zircon geochronology and Nd-Hf isotopes (Pastore et al. 2023), clay geochemistry and provenance (Bayon et al. 2024), and sand petrology and geochemistry (Garzanti et al. forthcoming).

The purpose of the present study is twofold, both methodological and regional. Following similar research in other large fluvio-deltaic systems (e.g., Garzanti et al. 2010, 2011, 2015a), we here scrutinize the grain-size dependent mineralogical and geochemical variability in sediment carried by the two main rivers of subequatorial Nigeria, the Niger and its largest tributary, the Benue (Fig. 1). Our aim is to obtain information on: 1) processes of clay, silt, and sand generation from diverse types of sources (wind-blown dust, soils and paleosols, siliciclastic units, crystalline bedrocks) in the subequatorial belt; 2) controls on the size distribution of detrital minerals, including settling equivalence, size inheritance, mechanical durability, chemical weathering, and chemical durability through multiple sedimentary cycles. We specifically focus on tectosilicates to investigate mechanisms of feldspar comminution and shed new light on the size dependence of quartz/feldspar and plagioclase/feldspar ratios, a long-standing petrological problem (Graham 1930; Odom et al. 1976; Basu 1985; Nesbitt et al. 1996; Dott 2003).

The regional issue we tackle is to determine the main source of the sediment delivered today to the Niger Delta. The separate compositional analyses of multiple size fractions using a range of techniques (optical microscopy, manual and semi-automated Raman spectroscopy, X-ray diffraction, elemental and isotope geochemistry) allows us to calculate in diverse independent ways the relative contribution from the Niger mainstem *versus* its largest Benue tributary for different size modes, from clay and silt entrained as suspended load to coarse sand transported as bedload. Inferences about changing sediment budgets through geological time are also made.

GEOMORPHOLOGICAL FRAMEWORK

Climate in Nigeria changes from hot semi-arid in the Sahel, to tropical savannah in the central part, and to tropical monsoonal in the coastal belt (Onafeso 2023). Rainfall increases steadily southwards from 0.5 - 0.75 m/a in the Sahel, to 1.2 m/a in the central region, and to > 2 m/a and even up to > 4 m/a along the coast, where the wet season lasts from March to October (Fig. 2A). Average annual temperatures range between 21°C and 27°C throughout the country, with excursions more pronounced during the day than among seasons (Eludoyin and Adelekan 2013). In the dry winter, the dusty northeasterly Harmattan wind blows from the Sahara over western Africa into the Gulf of Guinea.

The Jos Plateau in central Nigeria, with an average altitude of 1280 m above sea level peaking at 1829 m a.s.l. in the Shere Hills, is delimited by 300-m to 600-m-high escarpments around much of its boundary. Even higher elevations are reached along the Cameroon border in the east (Chappal

Waddi Mountain, 2419 m a.s.l.). In contrast, elevation is < 600 m a.s.l. in the north and west (Fig. 2B). Highlands correspond with uplifted metamorphic basement or igneous rocks, whereas sedimentary basins in the lowlands are filled with mostly fluvial siliciclastic deposits. Neoproterozoic or Jurassic granites form a rugged topography with inselbergs rising abruptly by hundreds of meters above the surrounding plains, whereas volcanic rocks exposed on the Jos Plateau are weathered to form 5-10 m-thick lateritic crusts (Zeese 1996). The southeastern uplands are low rounded hills capped by lateritic crusts and forest cover, and sedimentary domains in the south are thickly forested hills and swamps (Tijani 2023).

Vegetation varies with altitude and latitude (Fig. 2C), passing southward from savanna with only drought-resistant trees in the Sahel, to the sudanic zone characterized by corridors of forest trees along river valleys, to interlaced forest, savanna and grassland in central Nigeria, and finally to tropical moist forest near the coast (Gbadegesin et al. 2023). Soil types are varied depending on diverse factors (i.e., rainfall, internal drainage, substrate lithology). Kaolinite is the most common clay mineral in well-drained soils throughout Nigeria. Smectite occurs in drier northern areas and is predominant in soils with poor internal drainage formed on either pyroclastic deposits or basaltic lavas. Gibbsite is found only in very well-drained soils formed on the Jos Plateau (Zeese et al. 1994) or in the coastal region of southern Nigeria, where illite is virtually lacking because of high rainfall and most extensive chemical leaching (Gallez et al. 1975; Møberg and Esu 1991; Ojo et al. 2017).

THE NIGER RIVER

The Niger River (length ~ 4.200 km, basin area 2,100,000 km^2), the third largest in Africa after the Nile and the Congo (Welcomme and Dumont 1986), is here divided for convenience into four tracts: the Upper Niger from the headwaters in Guinea to the Inner Delta in Mali, the Sahelian Niger from the Inner Delta to the Nigerian border, the Middle Niger between the Nigerian border and the Benue confluence, and the Lower Niger downstream. Sourced in hot-wet subequatorial Guinea only 250 km east of the Atlantic coast, the Upper Niger forms an Inner Delta in the semi-arid lowlands of the Malian Sahel, where it loses much of its flow and nearly all of its sediment (Olivry et al. 1995). Downstream, the Sahelian Niger describes a great arc along the southern edge of the Sahara Desert, where bedload chiefly consists of sand recycled from eolian dunes and suspended load is rich in kaolinite and iron oxyhydroxides (Moussa et al. 2022).

In Nigeria, the Middle Niger flows along the Cretaceous Bida failed rift and receives sediment from western and eastern tributaries sourced in the Nigeria basement complex, which belongs to the Pan-African Trans-Saharan Belt and includes a core of Mesoarchean gneiss and Paleoproterozoic schist intruded by upper Neoproterozoic granites (Fig. 3; Ferré et al. 2002). In central Nigeria near Lokoja city (Fig. 1), the Middle Niger is joined by the Benue River (length 1400 km, basin area ~340,000 km^2), its largest tributary sourced in the volcanic highlands of Cameroon. The Benue flows westward along a Cretaceous failed-rift arm, receiving sediment from the Eastern Nigeria basement complex and Jurassic granites of the Jos Plateau in the north (Ngako et al. 2006) and from the Bamenda Massif in the southeast (Ibe 2020).

The annual water discharge of the Benue River (~100 Km^3) and other tributaries (e.g., Kaduna, ~20 Km^3) contributes to the large discharge of the Lower Niger (~270 km^3; FAO and IHE Delft 2020), which forms the largest delta in Africa (~19,000 km^2). The annual flood occurs in different months across the basin. In the Upper Niger River, discharge is high in the rainy summer and low in the dry winter, but the flow slows down sharply across the very low gradient and wide flooded area of the Inner Delta (Olivry et al. 1995). This *black flood* from upstream, characterized by clear desilted waters, crosses the Sahelian Niger only in winter, and thus reaches the Middle Niger well after the *white flood* characterized by waters laden with kaolinitic sediments that follows shortly the summer rain season (Ogunkoya 2023). The Benue River, instead, has only one flood season between May and October. Consequently, discharge in the Lower Niger peaks in November, with a slight rise in winter caused by floodwaters from the Upper Niger. The suspended sediment load of the Lower Niger is estimated as ~ 40 million tons/a (Hay 1998; Milliman and Farnsworth 2011).

METHODS

For this study of intrasample mineralogical and geochemical variability (i.e., compositional variability among size classes belonging to the same sample), we have specifically considered three samples of ~ 2 kg each collected manually on 20, 21, and 22 September 2010 from riverbanks in the vicinity of Lokoja city, from the Benue River 15 km upstream of the Niger confluence (6233), and from the Niger River 27 km upstream (6232) and 42 km downstream (6234) of the Benue confluence. On each sample, 15 grain-size classes were separately analysed with multiple mineralogical and geochemical techniques. Complementary information on another 18 sediment samples (Figs. 1 to 3; data from Pastore et al. 2023 and Garzanti et al. forthcoming) was used to evaluate size-dependent intersample mineralogical variability of Niger and Benue sediments (location and data provided in Appendix Tables A1 and A4).

Grain-Size and Mineralogical Analyses

The grain-size distribution of the three Lokoja samples was determined by both wet sieving (using 5 μm and 15 μm tissue sieves, and 32 μm, 40 μm, 63 μm, 80 μm, 125 μm, 180 μm, 250 μm, 355 μm, 500 μm, 1 mm, and 2 mm steel sieves) and laser granulometry using a Malvern Mastersizer 3000 particle size analyser. The results of laser analyses notably underestimated the amount of clay and will not be discussed hereafter. The < 2 μm (clay) and 2-5 μm fractions were separated by the settling-tube method adding sodium hexametaphosphate to avoid clay flocculation and a 3% hydrogen peroxide solution to remove organic matter. Previously obtained X-ray diffraction data for cohesive mud (< 15 μm) and clay (< 2 μm), illustrated in Bayon et al. (2024), were also considered.

Each size class between 2 μm and 500 μm was separated by centrifuging in sodium polytungstate into low-density (< 2.90 g/cm^3, "light" *L*) and high-density (> 2.90 g/cm^3, "heavy" *H*) fractions (Andò 2020). On the *H* fraction of each class, recovered by partial freezing with liquid nitrogen and mounted on glass slides, ~ 200 transparent heavy-mineral (tHM) grains were point-counted at appropriate regular spacing (Garzanti and Andò 2019). More than 5800 tHM were identified overall. All dubious grains and systematically all grains of fine silt size were checked by Raman spectroscopy.

On the *L* fraction of each class, and on the bulk (*L*+*H*) 0.5-1 mm and 1-2 mm classes, more than 1000 grains dispersed on a glass slide were identified on average by semi-automated Raman counting (~ 45,000 grains overall; Andò et al. 2011; Lünsdorf et al. 2019). Spectra were obtained by a confocal Renishaw Qontor™ spectrometer equipped with a Leica microscope, 532 nm solid state laser (~ 100 mW power), motorized stage, and autofocus, using 50 x LWD magnification and 10% laser power for 0.5 s (repeated for 35 cycles) on each grain. Baseline correction and spectra normalization were performed using Renishaw *Wire* software. Grains were identified using a *Matlab* routine that matches the obtained spectra with an in-house-built reference database of known mineral spectra (Andò and Garzanti 2014).

Goodness of fit was assessed by the correlation coefficient *r* (0, no match; 1, perfect match), accepting only values ≥ 0.7. Feldspars were identified as albite *vs.* Ca-plagioclase and as orthoclase *vs.* microcline by the position and width of the main Raman bands determined with *Origin* software. Tectosilicates have distinct Raman spectral features. The main Raman peak is at 464 cm^{-1} for quartz, at 513 cm^{-1} for K-feldspar, at 506–507 cm^{-1} for albite, and between 509 and 511 cm^{-1} for oligoclase, andesine, and labradorite (Freeman et al. 2008). Among K-feldspars, the width of all peaks increases, and the total number of vibration modes decreases, with increasing disorder in the crystalline structure. Well-ordered triclinic microcline is thus identified by three sharp peaks between 155 and 286 cm^{-1}, whereas orthoclase displays only two broader peaks in this frequency region.

Point-counting analyses by the Gazzi-Dickinson method were carried out on bulk samples (compositional classification after Garzanti 2019). Parameters used in this article include the **Q/F** and **P/F** ratios (Q, quartz; F, total feldspars; P, plagioclase). The **ZTR** index (sum of zircon, tourmaline, and rutile percentages relative to total tHM; Hubert 1962) expresses the durability of the tHM suite. The **T/(T+Amp)** (T, tourmaline; Amp, amphibole) ratio is introduced here as an index of recycling depurated from hydraulic-sorting effects (more durable tourmaline being more prone to survive multiple sedimentary cycles than equally dense amphibole).

The transparent heavy mineral concentration index **tHMC** is the percentage of tHM in the sediment, and the source rock density index **SRD** (in g/cm^3), defined as the weighted average density of extrabasinal terrigenous grains, is used as an estimator of the average density of source rocks in the absence of hydraulic effects (Garzanti and Andò 2007). The results of grain-size and mineralogical analyses are illustrated in Fig. 4 and Table 1, respectively. The complete mineralogical dataset is provided in Appendix Table A2.

Geochemical Analyses

Samples were treated using a sequential leaching procedure for quantitative removal of carbonates, Fe-oxide phases, and organic matter (Bayon et al. 2002). The concentration of selected major and trace elements was measured on powdered samples of each of 14 size classes (< 2 μm to 2 mm) after digestion by alkaline fusion (Bayon et al. 2009). Analyses were conducted with a Thermo Scientific Element XR sector field ICP-MS at the Pôle Spectrométrie Océan, using the Tm addition method and correction of isobaric interferences for the determination of REE abundances (Barrat et al. 1996). Analytical precisions were < 5%. The accuracy of measurements was assessed by analyzing two certified reference materials (BCR-2 and DR-N), yielding concentrations within 10% of reference values. Concentrations are not reported for Eu due to analytical issues during the session.

Nd isotopes were measured using a Thermo Scientific Neptune multi-collector ICP-MS at the Pôle Spectrométrie Océan, after Nd purification by conventional ion chromatography. Repeated analyses of a JNdi-1 standard solution gave $^{143}Nd/^{144}Nd = 0.512113 \pm 0.000009$ (2σ, n = 17), in agreement with the recommended value of 0.512115 (Tanaka et al. 2000) and corresponding to an external reproducibility of ± 0.18 ε (2σ). Epsilon Nd values were calculated using the present-day chondritic (CHUR) values $^{143}Nd/^{144}Nd = 0.512630$ and $^{147}Sm/^{144}Nd = 0.196$ (Bouvier et al. 2008). The results of geochemical analyses are illustrated in Table 2. The complete geochemical dataset is provided in Appendix Table A3.

GRAIN-SIZE DISTRIBUTION AND SIZE-DEPENDENT COMPOSITIONAL VARIABILITY

The three studied Middle Niger, Benue River, and Lower Niger sediment samples have a very similar grain-size distribution, a similarity that corroborates the consistency of the sampling criterion and assures a complete overview of size modes transported across these three main fluvial reaches. Sieve data indicate that all three samples consist of very coarse silt rich in clay and mostly very fine sand (Fig. 4). Their multimodal distribution resulted from collecting large (~2 kg) samples including more than a single sedimentation unit (*sensu* Otto 1938) and consequently comprising sediment transported in different modes at different depths of the fluvial channel and deposited at different settling velocities at different times.

All three samples show the same five modes, in clay (***C***, > 9ϕ), cohesive very fine to coarse silt (***fSi***, 9ϕ to 5ϕ; mean 20-23 μm), frictional very coarse silt (***cSi***, 5ϕ to 4ϕ; mean 55-56 μm), very fine to lower fine sand (***VFS***, 4ϕ to 2.5ϕ; mean 85-103 μm), and medium to very coarse sand (***CS***, < 2ϕ; mean 620-725 μm). The *cSi* frequency peak is higher than the *VFS* peak in the Middle Niger sample (modal class 40-63 μm) and lower than the *VFS* peak in the Benue sample (modal class 80-125 μm), where the > 250 μm fraction amounts to 5% only (*vs.* 15% in the Middle Niger sample). The Lower

Niger sample has intermediate characteristics (*VFS* peak slightly higher than the *cSi* peak and subdued *CS* peak; Fig. 4).

Intrasample Variability of Tectosilicate Proportions

Optical point-counting and semi-automated Raman-counting indicate that the Middle Niger sample is quartz-rich feldspatho-quartzose, whereas the Benue and Lower Niger samples are feldspar-rich feldspatho-quartzose. In all three samples, orthoclase prevails over plagioclase and plagioclase over microcline. Mica flakes (muscovite prevailing in the Middle Niger sample and biotite in the Benue and Lower Niger samples) and a few sandstone/siltstone, granitoid, and gneissic rock fragments occur (Fig. 5).

Tectosilicate proportions show similar grain-size trends in the three studied samples (Fig. 6). In the Middle Niger sample, cohesive silt (Q/F 2.9 ± 0.5, P/F 29 ± 3%), very coarse silt and very fine sand (Q/F 3.6 ± 0.6, P/F 38 ± 4%) are feldspatho-quartzose. Fine sand is quartz-rich feldspatho-quartzose (Q/F 5.7 ± 1.0, P/F 46 ± 8%) and quartz keeps increasing progressively from medium quartzose sand (Q/F 11 ± 4, P/F 40 ± 8%) to coarse and very coarse pure quartzose sand (Q/F 27 ± 12, P/F dropping from 29% to 13%; Table 1).

In the Benue sample, instead, cohesive silt (Q/F 1.1 ± 0.1, P/F 34 ± 1%), very coarse silt and very fine to fine sand (Q/F 1.8 ± 0.5, P/F 36 ± 4%) are feldspar-rich feldspatho-quartzose. Medium sand is feldspatho-quartzose to quartz-rich feldspatho-quartzose (Q/F 4.0 ± 0.4, P/F 34 ± 2%) and quartz increases further in quartz-rich feldspatho-quartzose coarse sand, where the Q/F ratio reaches 9 and the P/F ratio falls to 8% (5% in very coarse sand; Table 1).

The Lower Niger sample displays similar features as Benue sand. Cohesive silt (Q/F 1.4 ± 0.3, P/F 33 ± 1%) and very coarse silt to lower fine sand are feldspar-rich feldspatho-quartzose (Q/F 1.5 ± 0.3, P/F 45 ± 2%). Upper fine sand is feldspatho-quartzose (Q/F 2.2, P/F 30%) and medium to very coarse sand quartz-rich feldspatho-quartzose (Q/F 6.1 ± 2.3, with P/F ratio dropping to ≤ 25% and eventually falling to 0; Table 1).

In all three samples, the Q/F ratio increases gradually from the *fSi* mode to the *cSi* and *VFS* modes, and next sharply in the *CS* mode (Table 1). The P/F ratio is low in the *fSi* mode, reaches maximum in the *cSi* and *VFS* modes to fall in the *CS* mode (Fig. 6C). Quartz increases with grain size at the expense of feldspars, more rapidly relatively to plagioclase and less rapidly relative to K-feldspar. Although Raman-counting data do not show a clear grain-size dependence of the orthoclase/microcline ratio as observed in turbiditic sands of the Congo and Zambezi deep-sea fans (Garzanti et al. 2021a, 2022a), optical observations highlight the abundance of microcline with cross-hatched twinning in the coarsest tail of the size distribution of the studied samples (Fig. 5A, B, C), where the Q/F ratio tends to decrease (Fig. 6B). Granules are sandstone/siltstone, microcline-bearing granitoid rock fragments (Fig. 5G), gneiss (Fig. 5H), quartzite (Fig. 5I), or laterite and silcrete clasts (Fig. 5D, E, F).

Intrasample Variability of Heavy-Mineral Suites

Transparent-heavy-mineral concentration reaches maximum in the fine tail of the size distribution (3.0% and 5.0% in the 15-32 μm class of the Middle Niger and Benue samples, respectively, and 4.6% in the 32-40 μm class of the Lower Niger sample) and decreases rapidly in the coarse tail (0.1-0.9% in fine sand, 0.03-0.2% in medium sand) (Table 1). Zircon is markedly enriched in the fine tail along with rutile and monazite, whereas anatase becomes particularly abundant in the finest tail (2-5 μm class; Table 1). Epidote and titanite tend to decrease with grain size, whereas amphibole reaches its highest relative abundance in very fine to fine sand. Among minerals occurring in metasedimentary rocks, prismatic sillimanite and kyanite are more frequently observed in silt, andalusite in very fine to fine sand, fibrolitic sillimanite in fine to medium sand, and staurolite and garnet in medium sand.

Settling-Equivalence Analysis

Settling equivalence controls the size-dependent intrasample compositional variability in sediments deposited by tractive currents (Rubey 1933). The principles of settling-equivalence analysis are illustrated in detail in Garzanti et al. (2008). For the bulk sample, as well as for the *fSi, cSi*, and *VFS* modes that settled in laminar o quasi-laminar hydraulic regime, Stokes' formula predicts that size differences between detrital minerals in phi (ϕ) units ("size shifts") are half the difference between the logarithms of their submerged densities (McIntyre 1959). With larger grain sizes and settling velocities, viscosity becomes less and less important with respect to turbulence, and departures from Stokes' law progressively increase. The significantly larger size shifts for the *CS* mode must thus be calculated with empirical formulas (e.g., Cheng 1997).

Settling velocities are calculated to be 0.03 cm/s for the *fSi* mode, 0.2 cm/s for the *cSi* mode, 0.6 cm/s for the *VFS* mode, and 8.2 cm/s for the *CS* mode. At these settling velocities, amphibole or zircon are predicted to be, respectively, ~0.2 or ~0.6 phi class finer than quartz in the *fSi*, *cSi* and *VFS* modes, and ~0.3 or ~0.8 phi class finer than quartz in the *CS* mode.

Settling equivalence predicts a strong concentration of heavy minerals − in particular of densest zircon, monazite, and rutile − in the fine tail of the size distribution and the relative increase of less-dense heavy minerals (e.g., amphibole) in modal classes. Marked deviations from theoretical size-density relations however occur because of the co-existence in all three samples of multiple modes with different mineralogical composition. The coefficient of determination R^2, a useful measure of size-density sorting, is consequently low (Fig. 7). Moreover, because of quartz enrichment in coarser modes, most minerals are markedly finer than quartz than theoretically predicted.

This is particularly true for the most durable minerals, widely ranging in density from ~3.15 g/cm^3 for tourmaline to 4.65 g/cm^3 for zircon, which plot higher above the size-density curve than other common heavy minerals (e.g., hornblende, epidote, titanite) in all three samples (Fig. 7). Conversely, garnet tends to be coarser than expected. Opaque grains are concentrated both in the fine tail of the size distribution (where they are largely ultradense Fe-Ti-Cr oxides) and in the coarse tail (where they are largely less dense iron oxides-hydroxides derived from lateritic duricrusts).

Intrasample Variability of Chemical Composition

Intrasample geochemical variability is the consequence of mineral fractionation in different size classes, phyllosilicates in clay and fine silt, densest minerals in coarser silt, feldspars in very fine sand, and quartz in coarser sand (Fig. 8A). Mg and Sc are strongly concentrated in the finest tail of the size distribution (< 15 μm fraction) suggesting association with phyllosilicates, decrease in very coarse silt, and are very low in sand. In contrast, Ca, Sr, and Ba are much lower both in the finest (< 5 μm) and coarse (> 180 μm) tails of the size distribution than in intermediate size classes.

All elements preferentially concentrated in densest minerals (Zr, Hf, Y, REE and Th hosted in zircon, xenotime or monazite, and to a lesser extent Ti or Mn hosted in rutile or garnet) reach peak abundance in the fine tail of the size distribution (15-32 or 32-40 μm classes) (Table 2), i.e., ≤ 1ϕ-class finer than median bulk-sample grain size in agreement with the settling-equivalence principle. All analysed elements are depleted in the *CS* mode because of quartz dilution; most depleted are Mg and Ti, and least depleted are Ca, Sr and Ba hosted in feldspars.

Intrasample Variability of the Zr/Hf Ratio

The Zr/Hf ratio is 36 ± 1 in clay and 47 ± 4 in sand classes, matching the average values of chondrites (33–37; Weyer et al. 2002) and of zircon in common rocks (~ 47; Bea et al. 2006), as generally observed in sediments (e.g., Garzanti et al. 2022a). Unexpectedly low values, however, are reached in the class characterized by the highest Zr, Y and HREE concentration (Zr/Hf 25-28 either in the 15-32 μm or 32-40 μm class; Table 2 and Fig. 9). This indicates the presence of ultradense minerals with very low Zr/Hf ratio, possibly hydrothermal zircon (yielding a Zr/Hf ratio of 20-25 but even as low as 5; Wang et al. 2010; Bea et al. 2018) but also an yttrium-bearing mineral such as xenotime and niobium–tantalum oxides (e.g., columbite and wodginite from granitic pegmatites, yielding an average Zr/Hf ratio of 6-13 and 1-4, respectively; Černý et al. 2007). Columbite-group minerals are mined in Pan-African pegmatite veins across Nigeria and Fe-columbite is an accessory mineral in Jurassic alkaline granites of the Jos Plateau, where also wodginite and xenotime occur (Melcher et al. 2015).

Another anomalously low value (Zr/Hf 37) characterizes the 180-250 μm class of the Lower Niger sample (Table 2), which represents the fine tail of the *CS* mode and contains more xenotime than zircon (Table 1), as confirmed by the lowest Zr concentration (only 33 ppm) and the highest Y/Zr ratio (Fig. 8B). The Zr/Hf ratio in this class, therefore, is not controlled by zircon but by an Y-rich and Hf-bearing mineral (most plausibly pegmatitic xenotime) carrying a Zr/Hf signal close to the average chondrite value and notably lower than the average value of 45 reported for xenotime in Bea et al. (2006).

Intrasample Variability of ε_{Nd} Values

The ε_{Nd} values do not vary regularly with grain size, indicating that Nd-bearing minerals with different ε_{Nd} values occur in different proportions in different size classes. This is underscored by poor relations of ε_{Nd} with Nd (r = 0.25) and Th (r = 0.15), a couple of nearly perfectly correlated elements (r = 0.93) that provide a proxy for monazite content. Therefore, either monazite does not control the Nd budget in all size classes, or different ε_{Nd} signals are carried by distinct monazite populations characterized by different grain size.

The ε_{Nd} values, instead, correlate negatively with quartz (r = -0.58, 0.1% sign. lev.) and mildly positively with all analysed chemical elements, suggesting that quartz carries a more negative ε_{Nd} signal than monazite and other Nd-bearing detrital minerals. Although quartz is one of the purest minerals on Earth, impurities in the form of trace elements can be either incorporated into the crystal structure or bound to fluid or mineral inclusions. Even though REE cannot fit into the quartz lattice because of their crystal-chemical properties, quartz carries a non-negligible amount of Nd (0.5 ppm or more; Götze and Lewis 1994), hosted either in fluid inclusions (Götze et al. 2021) or in micro-inclusions of Nd-rich minerals (e.g., monazite; Odom and Rink 1989). The quartz contribution to the REE budget thus becomes significant in sand classes where quartz is overwhelming and heavy-mineral concentration extremely poor. The class richest in quartz (500-1000 mm, i.e., core of the *CS* mode) yielded the most negative values (ε_{Nd} -22 for the Middle Niger sample and ε_{Nd} -21 for the Benue and Lower Niger samples). Such strongly negative ε_{Nd} values, also reached in sand from the Zambezi catchment, Madagascar, and the Zambezi and Congo fans, are considered to be an indirect consequence of quartz durability (Garzanti et al. 2021a, 2022a, 2022b). Because quartz endures chemical attack during repeated cycles of weathering and diagenesis better than any other mineral including commonly metamict zircon, quartz grains bear greater chances to survive multiple recycling through geological time, and in cratonic settings are thus likely to carry a very strongly negative signal (ε_{Nd} down to -30 or even -40; figure 8 in Garzanti et al. 2021a) if originally released from Archean shields.

In the clay (< 2 μm) and finest mud (< 5 μm) fractions, where abundant phyllosilicates contribute significantly to the Nd budget, values are more negative in the Middle Niger (ε_{Nd} -18.41 ± 0.01) than in the Benue and Lower Niger samples (ε_{Nd} -11.7 ± 0.2 and -11.9 ± 0.3, respectively; Table 2). Grain-size fractions of the Lower Niger sample separated by centrifugation at 200, 1000, 2000, 3000, and 4000 revolutions per minutes were also analysed, and consistent ε_{Nd} values of -11.7 ± 0.1 were obtained for clay to fine silt (average grain size D_{50} ranging from 0.5 μm to 6.4 μm), decreasing to ε_{Nd} -15.2 ± 1.2 for the very-coarse-silt-sized bulk sample.

In silt classes between 5 μm and 63 μm − where Nd is largely contained in monazite −, ε_{Nd} values become more negative with increasing grain size (from -16 to -17 in the Middle Niger sample, and from -13 to -17 in the Benue and Lower Niger samples; Table 2), as monazite tends to decrease (Table 1). In very fine to lower fine sand (63-180 μm) − where quartz content is intermediate and monazite decreases rapidly with grain size as documented by rapidly decreasing Nd and Th (Table 2) − ε_{Nd} is close to bulk sample values (from -17 to -15 *vs.* -17 for the Middle Niger sample; from -13 to -12 *vs.* -13 for the Benue sample, and from -16 to -19 *vs.* -15 for the Lower Niger sample), confirming that the Nd budget is controlled by multiple minerals.

The ε_{Nd} values are most irregular in the fine tail of the *CS* mode (180-355 μm classes), rich in quartz but containing a few grains of both monazite and xenotime (Table 1). In the 180-250 μm class of the Lower Niger sample, the ε_{Nd} values reach as high as -8.9 (Table 2), pointing to the presence of monazite carrying a much less negative signal than quartz ($\varepsilon_{Nd} > -9$ *vs.* $\varepsilon_{Nd} < -20$) (Fig. 9). Such coarse monazite and xenotime grains are most plausibly derived from Pan-African pegmatites and/or Jurassic alkaline ring complexes of the Jos Plateau (Jefford 1962; Funtua and Elegba 2005). Finer and coarser monazite grains do not necessary share the same provenance and the same isotopic signal.

Intersample Mineralogical Variability

A comparison among sand samples collected along the Niger and Benue rivers and from tributaries draining the same geological domain (sample location and catchment geology indicated in Fig. 3; data from Garzanti et al. forthcoming provided in Appendix Table A4) offers additional clues to understand sediment-generation processes (Fig. 10). In the Middle Niger catchment, the Q/F ratio increases markedly from 5-11 in very fine sand to 56 in medium sand of the mainstem, and from 15 in coarsest silt to > 100 in medium and coarse sand of tributaries; the P/F ratio decreases from 28-51% in very fine sand to 0 in medium sand of the mainstem, and from 48% in coarsest silt to 0 in medium to coarse sand of tributaries. In the Benue catchment, the Q/F ratio increases from 1.3 in very fine sand to 2.9-3.7 in medium and coarse sand of the mainstem, and from 1.3 in fine sand up to 12 in coarse sand of tributaries; the P/F ratio decreases from 30% in fine sand to 13% in coarse sand. In Lower Niger samples, the Q/F ratio increases from 1.7 in very fine sand to 8-17 in medium sand, whereas the P/F ratio is unchanged (38% in very fine sand and 29-41% in medium sand).

In summary, the Q/F ratio increases systematically with increasing grain size by a full order of magnitude in Middle Niger and tributary sands and by a factor of ~ 3 in Benue and tributary sands. The P/F ratio falls drastically to 0 in medium to coarse sands in the Middle Niger catchment, and decreases progressively by a factor of ~ 2 from very fine to coarse sands in the Benue catchment. Micas are more common in very coarse silt to very fine sand, and heavy-mineral concentration decreases systematically with increasing grain size in all catchments. Among tHM, amphibole tends to decrease with grain size in Benue and tributary sands but does not show a consistent behavior in Niger and tributary sands (Appendix Table A4). Garnet and staurolite more frequently occur in coarser samples. Epidote, zircon, tourmaline, and other minerals do not show a clear trend.

Intersample Variability of ε_{Nd} Values

Middle Niger sediments collected upstream of Lokoja city yield values becoming more negative from very coarse silt (ε_{Nd} -16.4) to very fine sand (ε_{Nd} -19.8) and fine/medium sand (ε_{Nd} -22.5), indicating strong grain-size control (data from Pastore et al. 2023 provided in Appendix Table A4). Instead, Benue River sediments collected from the Niger confluence to 360 km upstream yield remarkably consistent values from very coarse silt to coarse sand (ε_{Nd} -12.0 ± 0.6). Lower Niger sediments collected shortly downstream of Lokoja city display intermediate values, ranging from ε_{Nd} -11.6 to ε_{Nd} -14.7 in very coarse silt to medium sand independently of grain size. Isotopic values increase markedly in sand of deltaic distributaries (ε_{Nd} -18.7 ± 0.4), reflecting recycling of quartz-rich Cenozoic deposits derived in larger proportion from the upper reaches of the Niger mainstem (Pastore et al. 2023).

These observations confirm that a more negative ε_{Nd} signal is carried by largely recycled quartz grains (most abundant in Middle Niger sand and concentrated in coarser sediment fractions) than by other detrital components derived in greater proportions directly from Pan-African basement rocks (more abundant in Benue sand and concentrated in finer sediment fractions).

CONTROLS ON SIZE-DEPENDENT COMPOSITIONAL VARIABILITY

This section discusses and speculates on the relative role played by different controls on the size-dependent composition of Niger sediments. Although each of the three studied samples consists of multiple modes, size-density sorting still explains much of the intrasample mineralogical variability of heavy-mineral suites (e.g., strong concentration of zircon and monazite in the 15-32 µm and 32-40 µm classes; Table 1 and Fig. 7) and consequently much of the strong intrasample geochemical variability (e.g., strong concentration of Zr, Hf, Y, REE, and Th in the same classes; Table 2). Size relations among quartz and feldspars, instead, are largely independent of hydrodynamic processes because of similarly low tectosilicate densities, narrowly ranging from 2.56 g/cm^3 for orthoclase and microcline to 2.67 g/cm^3 for andesine.

The long-reported increase of the Q/F ratio with grain size from a variety of sand and sandstone suites has been variously explained by original size differences in source rocks (Hayes 1962), lower durability of cleavable feldspars to mechanical impacts (Odom 1975; Garzanti 1986), chemical weathering (Basu 1976), polycyclicity (Dott 2003), or a combination thereof (Charles and Blatt 1978). High-resolution compositional analysis of the three Lokoja samples indicates that feldspar-grain size relations are complex (von Eynatten et al. 2012, 2016), pointing at different controls for the five identified size modes generated from different sources (i.e., wind-blown dust, pedogenic duricrusts, sedimentary deposits, or diverse igneous and metamorphic bedrocks) in different physical (weathering-limited) *vs.* chemical (transport-limited) erosional regimes.

Mechanical Effects

Mechanical abrasion can reduce the size of cobbles and pebbles efficiently − at different rates depending on clast lithology − during transport in gravel-bed mountain rivers (Kodama 1994; Attal and Lavé 2009). Size reduction, however, becomes rapidly less effective with decreasing pebble size in less steep sand-bed channels (Kuenen 1956) and mechanical abrasion has long been demonstrated unable to significantly modify the size and shape of sand grains during even very-long-distance transport in low-gradient rivers (Russell 1937; Shukri 1950; Kuenen 1959; Breyer and Bart 1978; Garzanti et al. 2012a). Mechanical effects, therefore, can hardly be held responsible for the tectosilicate-size relations observed in the Niger and Benue rivers, which are characterized by invariably low steepness indices (Fig. 11).

Among tHM, staurolite and garnet occur more frequently in the *CS* mode of all three Lokoja samples as in coarser fluvial sands collected across Nigeria, which can be ascribed to their original large crystal size in metamorphic basement rocks coupled with their hardness and thus mechanical durability (Resentini et al. 2018; Feil et al. 2024). Conversely, good cleavability may explain the tendency of amphibole to concentrate in finer fluvial sediments (Kelling et al. 1975; Garzanti et al. 2015b). Comminution of mica flakes explains the concentration of phyllosilicates in the *fSi* mode as in finer-grained sediment samples collected across Nigeria.

Weathering

Chemical weathering is strong in subequatorial Nigeria, as indicated by the extremely high indices of the clay fraction (CIA 95 ± 3) mostly consisting of kaolinite (59-69% of clay minerals in the three Lokoja samples; Table 1). Indices such as the CIA (Nesbitt and Young 1982), however, are markedly size-dependent and may reflect depletion in mobile elements inherited from previous sedimentary cycles (Garzanti and Resentini 2016).

The CIA indices could not be determined for the silt and sand classes analysed in this study because they were digested by alkaline fusion to maximise the accuracy of trace-element data. A comparison among sediment samples collected across Nigeria shows that the CIA is notably lower in cohesive silt than in clay (CIA ~ 75 in the < 15 μm fraction of Ka tributary sediment) and systematically low in sand generated in the Middle Niger (CIA 57 ± 3) and Benue (CIA 54 ± 3) catchments and supplied to the Lower Niger (CIA 54 ± 2; data from Garzanti et al. forthcoming provided in Appendix Table A4). Weathering effects, overwhelming for the clay mode, are thus indicated to be strong for the *fSi* mode and to become progressively weaker in the *cSi* and *VFS* modes. Petrographic observations, however, indicate that weathering intensity is quite significant also for the *CS* mode, which contains extensively corroded quartz grains, selectively altered feldspars with hematite-stained clay "plasma" penetrating along cleavage and twinning planes (Fig. 5A, B, C), and ferricrete and silcrete clasts (Fig. 5D, E, F).

Going beyond such general observations to assess the impact of weathering on feldspar-grain size relations is however difficult. A comparison across cratonic southern Africa shows that sand from the Niger catchment in Nigeria has a notably lower P/F ratio (P/F 27 ± 16%; Appendix Table A4) than Limpopo, Zambezi, or Orange river sands, where P/F consistently remains in the 60 ± 5% range (Garzanti et al. 2014a). Such a higher range of values also characterizes river, beach, and eolian sands in hyperarid Namibia (Garzanti et al. 2014b) and dominantly first-cycle river and beach sand in arid southern Angola (P/F 64 ± 7 from 15°S to 13°S), passing to lower values with increasing humidity in central (P/F 44 ± 8 from 13°S to 11°S) and northern Angola (P/F 40 ± 10 from 11°S to 7°S; Garzanti et al. 2018). In river sand, the Q/F ratio increases northward from 1.2 ± 0.2 in southern Angola to 1.9 ± 0.7 in central Angola, and to 7 ± 4 in northern Angola, where quartz is however extensively recycled.

These observations corroborate the widely established order of resistance to chemical weathering quartz > K-feldspar > plagioclase (Blatt 1967a; Nesbitt et al. 1997). Weathering effects can thus explain the progressive increase in the quartz/feldspar ratio with grain size in Niger sediments, as well as the dearth of plagioclase in the coarse tail of the size distribution. They may also explain the increase of the P/F ratio from the more intensely weathered *fSi* mode to the *cSi* and *VFS* modes generated by more physical than chemical processes (von Eynatten et al. 2016; Table 1).

Weathering effects are less evident for tHM suites. Among chemically labile ferromagnesian minerals, amphibole reaches maximum in the *VFS* mode, being notably depleted in both *fSi* and *CS* modes (Table 1). Pyroxene and olivine grains are few and their relative abundance does not show size-dependence.

Size Inheritance

The size of any detrital mineral in a daughter sediment is limited by the availability of crystal sizes in the parent rocks (Morton and Hallsworth 1999; Feil et al. 2024). According to Blatt (1967b, 1970), quartz grains released from granitoids and gneisses are 35-40% in the 1-4 mm range (~ 670 µm on average; ~ 500 µm if only monocrystalline quartz is considered), coarser than in schists (~ 440 µm), and much coarser than in sedimentary rocks (~ 60 µm on average, assuming that quartz is contained 30% in mudrocks, 65% in sandstones, and 5% in hybrid carbonates). In granitoid rocks, microperthite was observed to be coarser than orthoclase, orthoclase than microcline, and microcline than plagioclase; feldspar crystals in bedrocks resulted to be one or two phi classes larger than quartz on average (~ 0 ϕ *vs.* ~ 1.5 ϕ), and quartz several phi classes larger than apatite and zircon (Feniak 1944). Blatt (1985) reckoned that mudrocks contain 5-7% feldspars and sandstones 12%, and thus that more widespread mudrocks contain at least as large a volume of feldspar as sandstones.

These estimates suggest that the size of tectosilicates is typically reduced by an order of magnitude by physical and/or chemical processes during sedimentary cycles, amply sufficient to blur any size inheritance in most cases: although coarser than quartz in granitoid source rocks, single feldspar grains end up being typically finer than quartz in sedimentary rocks. The very large size of feldspar crystals in rock fragments (e.g., Fig. 5G), however, allows us to safely ascribe to size inheritance the decrease of the Q/F ratio in the coarsest classes of Middle Niger and Benue samples (Fig. 6B).

Anomalous size-density relations have been ascribed to size inheritance for virtually all heavy minerals and most commonly for garnet (Feil et al. 2024), although mixing of sediment with more distal *vs.* more proximal sources (e.g., figures 22 and 26 in Garzanti et al. 2015a; figures 9 and 10 in Resentini et al. 2018), density differences within isomorphous series (Krippner et al. 2015, 2016), or abundance of fluid or solid inclusions (Garzanti et al. 2008; Schönig et al. 2021) commonly represent concurrent causes. Detrital tourmaline from pegmatites can be notably coarser than tourmaline from metamorphic rocks (von Eynatten and Dunkl 2012), and epidote and titanium oxides derived from granular aggregates grown in source rocks during diagenesis or very-low grade metamorphism are commonly of silt size (figure 8 in Garzanti et al. 2011).

Size inheritance can explain why garnet, staurolite and aluminum silicates grown in medium/high-grade metapelites and pegmatite-derived tourmaline are more frequently observed in the coarse tail of the size distribution (Table 1), whereas recycled ZTR minerals are markedly concentrated in the fine tail (Fig. 8) and titanium oxides (anatase and subordinately brookite) in the finest 2-5 µm class (Table 1). Prismatic sillimanite is also concentrated in the *fSi* mode.

Size inheritance is most manifest in the *CS* mode, which does not only contain unexpectedly low percentages of lower-density amphibole and unexpectedly high percentages of denser garnet and staurolite, but also rare densest minerals − including soft barite and xenotime, relatively soft monazite and titanomagnetite, and very hard corundum – that evidently occur in equally large or larger sizes in Nigerian source rocks. Intersample comparisons confirm the tendency of garnet and staurolite to concentrate in coarser samples, and of titanium oxides and epidote to concentrate in finer samples.

Recycling

According to Blatt and Jones (1975), sedimentary rocks − two-thirds mudrocks, one fourth sandstones, one tenth carbonates − account for two-thirds of the rocks exposed at the Earth's surface; half of them are younger than Jurassic, indicating a lognormal decay of outcrop area with a half-life of ~ 130 Ma. Such a high recycling rate implies that large rivers flowing across intracratonic, foreland, or retroarc sedimentary basins are supplied with, and entrain a conspicuous proportion of polycyclic grains.

Recycling is *per se* a physical process that, in a weathering-limited denudation regime, can only reproduce the mineralogy of parent siliciclastic units in daughter sediments (e.g., unchanged quartz/feldspar ratio; Nesbitt and Young 1996; Garzanti 2017). In the case of rivers draining subequatorial intracratonic basins such as the Niger or the Congo, however, strong weathering effects in the current climatic regime are superposed onto the effect of chemical dissolution during previous sedimentary cycles (Garzanti et al. 2020). Disentangling textural, mineralogical, and geochemical properties acquired in the last sedimentary cycle from those inherited from a variety of polycyclic siliciclastic parent rocks thus becomes a very challenging task.

The Middle Niger and Benue rivers drain areas with similar precipitation (Fig. 2A), climate (Fig. 2C), and geomorphological characteristics (Figs. 2B and 11). Both rivers flow across Cretaceous rift-related basins (Fig. 3), but the Niger mainstem also drains the Iullemeden-Sokoto and Taoudeni sedimentary basins in the upper reaches and carries substantial sand recycled from Saharan dunes. All size classes of Middle Niger sediment are consequently much richer in recycled quartz than Benue sediment (Fig. 6A).

Heavy-mineral suites confirm the higher proportion of recycled detritus in Middle Niger sediment, including lower tHMC and notably higher ZTR and T/(T+Amp) indices in all size classes but one (Table 1). In the Middle Niger sample, both ZTR and T/(T+Amp) indices are higher both in the fine and coarse tails of the size distribution than in the modal classes (Fig. 12), suggesting that the percentage of recycled detritus is higher for the *fSi* and *CS* modes than for the c*Si* and *VFS* modes.

Intersample comparisons confirm that sand of the Middle Niger and its tributaries is much richer in quartz and has lower tHMC and notably higher ZTR and T(T+Amp) indices than sand of the Benue River and its tributaries (data from Garzanti et al. forthcoming provided in Appendix Table A4).

Rough best fit calculations based on tectosilicate proportions (assuming Q/F 1 and P/F 50% for the first-cycle endmember, and Q/F 10 and P/F 10% for the recycled endmember) indicate that Middle Niger sediments are mostly recycled (from 70 ± 10% for the *CSi* and *VFS* modes to > 90% for coarser sand), whereas Benue sediment is mainly derived directly (70 ± 5% of the *CSi* and *VFS* modes and ~50% of coarser sand) from the Eastern Nigeria basement complex, Jos Plateau, Bamenda Massif and Cameroon Volcanic Line, the rest being accounted for by detritus recycled from sedimentary strata of the Benue failed-rift trough.

The relative amounts of recycled *versus* first-cycle detritus can be independently estimated based on SRD and tHMC indices (assuming tHMC 4 and SRD 2.70 for the first-cycle endmember and tHMC 0.1 and SRD 2.65 for the recycled endmember; Garzanti et al. 2009). These calculations confirm that recycled sediment prevails in the Middle Niger, whereas first-cycle detritus prevails in the Benue and Lower Niger. Recycled detritus notably increases again across the Niger Delta (Pastore et al. 2023).

Processes of Clay Generation

Clay transported by the Niger River and its tributaries has diverse origins, both within and outside the drainage basin, as isotopic signatures suggest that Saharan dust may account for up to 40 ± 20% of the finest sediment load exported to the Gulf of Guinea (Bayon et al. 2024).

All along the Niger River, clay minerals are dominantly kaolinite largely derived from well drained subequatorial soil profiles, where mobile alkali and alkaline-earth elements have been extensively leached out from the regolith (CIA index 95 ± 3 for river clays across Nigeria; Bayon et al. 2024). Not all kaolinite, however, is generated in modern climatic conditions, but much has to be detrital and eroded from paleosols occurring throughout Nigeria (e.g., Zeese 1991; Ojo et al. 2011, 2017). Middle Niger clay also contains common smectite generated in the less extensively leached vertisols that characterize the wetter part of the Sahel from southern Mali to northeastern Nigeria (Møberg and

Esu 1991; Deckers et al. 1995). Benue and Lower Niger clay, instead, contains common mica/illite (Table 1), indicating relevant contribution from physical erosion of metamorphic basement rocks. During ferralitic weathering, titanium minerals (e.g., ilmenite) typically alter to leucoxene, with anatase as a final product in the clay fraction (Muggler et al. 2007). The common presence of Ti oxides in clay, as revealed by SEM analyses throughout the Niger catchment (Bayon et al. 2024), thus indicate reworking of intensely weathered soils and paleosols.

In addition to clay generated within the catchment, large quantities of eolian dust are deflated from the Sahara Desert, and mostly from the Chad basin including the Bodélé Depression, a major source of Harmattan dust haze (Bristow et al. 2009; Gherboudj et al. 2017). Clay minerals originated in the Sahel belt, including the area once occupied by paleolake Megachad, are dominantly kaolinite (illite/kaolinite ~0.1; Claquin et al. 1999; Caquineau et al. 2002; Scheuvens et al. 2013), indicating inheritance from intensely weathered lateritic soils developed at older times under humid subequatorial climate (Drake et al. 2022).

Processes of Silt Generation

The *fSi* mode of the three Lokoja samples displays lower Q/F and P/F ratios (Fig. 6) and notably higher ZTR and T(T+A) indices (Fig. 12) than the more abundant *VFS* mode. These four properties commonly characterize finer-grained siliciclastic layers in ancient sandstone suites (Odom et al. 1976) and can be plausibly ascribed to size reduction of feldspars and selective breakdown of plagioclase and more labile heavy minerals by the combined effects of mechanical comminution, chemical weathering in soils, and especially intrastratal dissolution through multiple sedimentary cycles (Dott 2003). The concomitance of these features suggests that the *fSi* mode is largely recycled from soils developed on siliciclastic rocks in lowland areas. The strong concentration of anatase and subordinately brookite in the finest tail of the size distribution, documented by combined optical and Raman analyses (Table 1), confirms extensive reworking of weathered soils and paleosols.

The low Q/F ratio is at odds with the pure quartzose composition of Saharan sediments (Pastore et al. 2021), ruling out − in contrast with the clay mode – a significant contribution from Saharan silt blown by Harmattan winds towards the Gulf of Guinea.

In the *cSi* mode, both Q/F and P/F ratios begin to increase (Fig. 6), while ZTR and T/(T+Amp) indices start to decrease rapidly (Fig. 12); amphibole increases, and titanium oxides become rare (Table 1). These features indicate increasing influence of physical erosion and higher proportions of detritus derived first-cycle from the Nigeria basement complex, and thus intermediate conditions between those leading to generation of the *fSi* and *VFS* modes.

Processes of Sand Generation

The *VFS* mode has similar or slightly higher Q/F and P/F ratios than the *cSi* mode (Fig. 6) but much lower ZTR and T(T+A) indices (Fig. 12). The percentage of recycled detritus is thus notably less than for silt especially for Benue sand, largely generated by erosion of the Eastern Nigeria basement complex and also containing clinopyroxene, orthopyroxene, and olivine derived from the Cameroon Volcanic Line (Garzanti et al. forthcoming).

Remarkable compositional differences are displayed by the *CS* mode, including the highest Q/F and lowest P/F ratios (Fig. 6), together with high ZTR and T/(T+Amp) indices especially in Middle Niger and Lower Niger samples (Fig. 12) where the *CS* mode is more significant (Fig. 4). These features, together with the occurrence of coarse tHM minerals relatively resistant to diagenetic dissolution (tourmaline, garnet, staurolite, andalusite, monazite, xenotime, corundum), suggest that the *CS* mode is derived from recycling of coarser-grained siliciclastic units widely exposed in the Iullemeden-Sokoto and Bida basins, with direct or indirect contribution from Pan-African pegmatites.

Relatively low CIA indices of river sand across Nigeria (Garzanti et al. forthcoming) indicate that sand generation mainly occurs by physical erosion in largely temperate-dry climatic conditions (Fig.

2C). The drastic decrease in plagioclase in the CS mode is thus mainly ascribed to selective diagenetic dissolution inherited from siliciclastic source rocks.

PROVENANCE BUDGETS: MIDDLE NIGER *VS.* BENUE

The proportion of sediment supplied by the Middle Niger *versus* its Benue tributary can be calculated in different ways, directly from gauged data (NEDECO 1961) or indirectly by forward-mixing calculations based on mineralogical, geochemical, or geochronological data (Garzanti et al. 2012b; Resentini et al. 2017). Because of significant size-controlled compositional variability, forward mixing calculations were made also separately for each of the five identified size modes (Table 3).

Clay, Silt, and Sand Budgets based on Mineralogical Data

Lower Niger clay has less kaolinite, much more illite, and much less smectite than Middle Niger clay (Table 1), and is quite similar to Benue clay with an even lower kaolinite/illite ratio, thus indicating overwhelming (~100%) clay supply from the Benue River.

For the *fSi* mode (average of 2-5 µm, 5-15 µm, and 15-32 µm classes), Raman-counting data of the low-density *L* fraction and optical + Raman point counting of the dense *H* fraction indicate prevalent supply from the Benue River but with significant contribution from the Middle Niger (~ 30% for both *L* and *H* fractions). The same proportion ~ 70:30 is calculated based on X-ray diffraction results on the < 15 µm fraction (data from Bayon et al. 2024). Data for the *cSi* mode (average of 32-40 µm and 40-63 µm classes) confirm prevalence of Benue supply, with contribution from the Middle Niger calculated to be lower for the *L* fraction (~ 5%) than for the *H* fraction (~ 30%; Table 3).

Benue contribution resulted to be overwhelming for the *VFS* mode (average of 63-80 µm, 80-125 µm, and 125-180 µm classes). Middle Niger contribution, undetected for the *L* fraction and minor for the *H* fraction (~ 5%), increases for the *CS* mode (average of classes > 250 µm; ~ 10% for the *L* fraction and dominant for the *H* fraction that, however, represents only ~ 1‰ of total sediment).

Calculations based on integrated data on the *L* and *H* fractions indicate that Middle Niger contribution decreases from ~ 30% for the *fSi* mode to ~ 12% for the *cSi* mode, it is undetected in the *VFS* mode, but significant again for the *CS* mode (Table 3). Calculations based on bulk-sediment data indicate a Middle Niger contribution ≤ 10%.

Sediment Budgets based on Elemental Geochemistry

Forward mixing calculations based on major and trace elements can be carried out in a variety of ways, for each single grain-size class, for each mode or for bulk samples, and for each element, for a string of selected elements or for all elements. In our calculations, we chose not to consider chemical elements preferentially hosted in densest minerals (e.g., Y, REE, Th, Zr, and Hf), because hydraulic-sorting effects make them vary by up to more than one order of magnitude among samples and by up to more than two orders of magnitude among different size classes of the same sample (Table 2). Nevertheless, calculations made class by class gave inconsistent results. More reliable calculations based on bulk-sample data and carried out according to different criteria confirm dominant sediment supply from the Benue River (Table 3).

Sediment Budgets based on Isotope Geochemistry

Forward mixing calculations based on ε_{Nd} and ε_{Hf} (data from Pastore et al. 2023 and Bayon et al. 2024 provided in Appendix Table A3) are better performed separately, because Nd and Hf budgets are not necessarily coincident being different the main carriers of Nd (mostly monazite) and Hf (mostly zircon). Although not particularly robust, being based on one compositional parameter only, calculations consistently indicate predominant supply from the Benue River, varying from a minimum of 52% to a maximum of 100% depending on the considered chemical element, endmembers, and sediment fractions. Best estimates of Benue contributions are ~ 83% (ε_{Nd}) for the bulk sample, ranging between 86% (ε_{Hf}) to 98% (ε_{Nd}) for clay and between 81% (ε_{Hf}) and 96% (ε_{Nd}) for sand. Calculations carried out class by class suggest overwhelming Benue supply for cohesive mud (< 32 μm) but give inconsistent results − ranging from 0% to 100% − for very coarse silt and sand classes.

Zircon Budget

The close similarity of U-Pb age spectra of Benue and Lower Niger sands (Fig. 13) indicate that zircon grains in the Lower Niger are supplied in much greater proportion by the Benue River (≥ 88%) than by the Middle Niger (≤ 12%), which carries notably more Paleoproterozoic zircon grains (24 ± 1%) than Benue (7 ± 2%) and Lower Niger (9 ± 4%) sands (data and calculations illustrated in Pastore et al. 2023). Because zircon concentration is similar (~ 1‰) in sand carried by the Benue and Middle Niger, zircon-age data confirm that the Benue River supplies most Lower Niger sand.

Sediment Fluxes through Time

Based on gauging data collected before the closure of most major dams, annual suspended load and bedload were estimated to be 4.6 and 0.3 million tons for the Middle Niger and 11 and 0.6 million tons for the Benue River, respectively (NEDECO 1961). These figures imply that Benue suspended load and bedload were higher than in the Middle Niger by factors of 2.4 and 2.0 − bedload accounting for 5-7% of total load − and that annual sediment yields and average erosion rates are an order of magnitude greater in the Benue catchment (34 tons/km^2 and 0.013 mm) than in the Niger mainstem (3 tons/km^2 and 0.001 mm).

A wide range of calculations based on independent methods and datasets converge to indicate dominant Benue supply to the Niger Delta (85 ± 12%; Table 3). Dominance of Benue supply, however, may be a relatively recent phenomenon induced by climate change and subsequently enhanced by human activities. In the last half century, Middle Niger load has been markedly reduced by impoundment in major artificial reservoirs (Abam 1999), including Kainji Lake in western Nigeria (closed in 1968; Ogunkoya 2023), the hydropower Jebba Dam ~100 km downstream (closed in 1984; Yue et al. 2022) and the Shiroro Lake on the Kaduna River (closed in 1990; Daramola et al. 2022).

Both artificial traps and natural traps to sediment transport exist in the Upper Niger catchment, including Markala Dam (closed in 1947 on the mainstem) and Sélingué Dam (closed in 1982 on the Sankarani tributary), and nearly all sediment generated in Guinea and southwestern Mali is dumped in the Inner Delta (Pastore et al. 2023).

Because of extensive evaporation in the presently dry climate, between 32% (driest years) and up to 47% (wettest years) of Upper Niger flow is lost in Inner Delta marshlands. Rainfall shortage, drought, and enhanced desertification determined an annual decrease in Upper Niger runoff of 20% during the 1970s and of 46% during the 1980s. Runoff kept decreasing also in the following years, as reflected in lower discharge during the annual floods, large reduction of groundwater storage, and degradation of hydrological resources (Olivry et al. 1995).

Because of the strongly negative water budget across the Sahel, the annual flow entering Nigeria was reduced from ~ 25 km^3 to 13.5 km^3 during the 1980s (FAO 1997). The combined impact of human activities and climate change over the last half century has been so extensive that, in June 1985, the Niger River dried up completely in Niger for the first time in history, and the flow recorded in 2003 was among the lowest in 50 years (Olomoda 2012). Conversely, flood events are expected to increase in magnitude for the Benue River (Olayinka-Dosunmu et al. 2022).

Sharply decreasing sediment fluxes in the last decades as a consequence of aridification in the Sahel suggest that sediment loads in the more humid past were significantly greater than the gauged annual suspended load of ~ 17 million tons for the Middle Niger and Benue River combined (Adegoke et al. 2017), and plausibly closer to ~ 40 million tons (Hay 1998; Milliman and Farnsworth 2011). These two values correspond to conservative figures for annual sediment yield (8 and 19 tons/km^2) and erosion rate (0.003 and 0.007 mm) averaged across the entire catchment, still compatible with the accumulation of ~ 500.000 km^3 of sediment in the Niger Delta that actively prograded since Eocene times (Hospers 1965; Tuttle et al. 1999; Reijers 2011).

It is thus entirely plausible that the Middle Niger used to be the most prominent sediment supplier to the Niger Delta in earlier times, starting from Oligocene drainage stabilization and until the latest Pliocene, when clastic fluxes dropped in response to the aridification that dried up Sahelian Niger tributaries sourced from the Hoggar swell (e.g., Wadi Dallol Bosso; Chardon et al. 2016; Grimaud et al. 2018). This is consistent with ε_{Nd} and ε_{Hf} values becoming more strongly negative in sand downstream the Lower Niger and in the Niger Delta, where quartz and ZTR minerals increase, and small populations of detrital zircons with Paleoarchean (Leonian), Mesoarchean (Liberian) and Neoarchean U-Pb ages reappear attesting to extensive reworking of sand supplied in larger proportions by the Middle Niger at earlier times of wetter climate (Pastore et al. 2023).

CONCLUSIONS

The dissection in 15 grain-size classes of three sediment samples characterized by very similar grain-size distribution and deposited by the Middle Niger, Benue and Lower Niger rivers in central Nigeria allowed us to probe into the complexities of sediment-generation processes in cratonic subequatorial western Africa. Diverse size modes (clay, fine cohesive silt, very coarse frictional silt, very fine sand, coarse sand) are supplied in different proportions from different sources (wind-blown dust, soils and paleosols, siliciclastic units, igneous and metamorphic bedrocks).

Kaolinite-dominated clay is derived partly from extensively leached soils and paleosols, developed during both present and past phases of hot and wet climate, but also partly from Saharan sources outside the Niger catchment. Feldspatho-quartzose (Middle Niger) to feldspar-rich feldspatho-quartzose (Benue and Lower Niger) fine silt (*fSi* mode) is largely derived from soils developed on siliciclastic rocks in the lowlands, as also supported by strong concentration of anatase. Decreasing ZTR minerals and increasing amphibole indicate that the proportion of first-cycle detritus from basement rocks increases from very coarse silt (*cSi* mode) to very fine sand (*VFS* mode). Relatively low CIA indices of river sand across Nigeria suggests that sand is produced mainly by physical erosion in temperate-dry climatic conditions. The signature of coarse sand (minor *CS* mode), characterized by highest Q/F, lowest P/F, and high ZTR and T/(T+Amp) indices, suggests recycling of coarser-grained siliciclastic units widely exposed in the Iullemeden-Sokoto Basin and Nigerian failed-rift troughs.

The peculiar trace-element or isotopic signatures (e.g., high HREE, very low Zr/Hf, less negative ε_{Nd}) of the fine tail of the *cSi*, *VFS*, or *CS* modes points at the presence of rare ultradense grains including monazite, xenotime and columbite-group minerals derived from Pan-African pegmatites and Jurassic alkaline ring complexes of the Jos Plateau.

The Q/F ratio markedly increases with increasing grain size both in different classes of the same sample (Fig. 6B) and in different sand samples collected across Nigeria (Fig. 10A). The long-standing petrological problem of feldspar-grain size relations has no simple explanation. Because feldspars are larger than quartz in granitoid source rocks, lower mechanical durability of cleavable feldspars and lower chemical durability of plagioclase must play a role. The sharp decrease of the P/F ratio in both fine silt and coarse sand modes (Fig. 6C), inferred to contain a larger percentage of recycled detritus, points at accumulation of these effects through multiple sedimentary cycles, and specifically at partial dissolution and selective replacement of less durable feldspars in siliciclastic source rocks during the intervening diagenetic stages.

Numerous sets of independent provenance calculations based on tectosilicate proportions, heavy minerals, elemental geochemistry, isotope geochemistry and detrital zircon geochronology, together with gauged sediment fluxes, converge to indicate that the major Benue tributary supplies 85 ± 12% of the sediment reaching the Niger Delta today (Table 3). Dominance of Benue supply, however, may be a relatively recent phenomenon, induced by climate change most severely affecting the Middle Niger catchment and subsequently enhanced by closure of major dams on the Niger mainstem and its major tributaries. While the Sahel is becoming drier, flood events are expected to increase in magnitude for the Benue River. The coherent change of diverse compositional parameters along the

Lower Niger and in the Niger Delta [i.e., increase of Q/F, ZTR and T/(T+Amp) indices, decrease of P/F and ε_{Nd} values, and re-appearance of Archean zircon grains] testifies to extensive local reworking of sand supplied in significantly larger proportions by the Middle Niger in the wetter past, before clastic fluxes dropped markedly in response to aridification of the Sahel.

ACKNOWLEDGMENTS

Brume Overare is warmly thanked for providing samples of Nigerian river sediments and for discussions on the geology and geomorphology of Nigeria. X-ray diffraction analyses were carried out by Pedro Dinis. Funding was contributed by Project MIUR – Dipartimenti di Eccellenza 2023–2027, Department of Earth and Environmental Sciences, University of Milano-Bicocca. The manuscript benefited greatly from careful handling by JSR Editor Dustin E. Sweet, advice provided by Associate Editor Gary Hampson, and meticulous constructive reviews by anonymous and Hilmar von Eynatten, who generously provided very precious insight on key mineralogical and geochemical issues.

SUPPLEMENTARY MATERIAL

Full information on the Middle Niger, Benue, and Lower Niger samples collected in the vicinity of Lokoja city is provided in Appendix A, to be found in the online version of this article at http://dx.doi.___________ : Table A1 includes the location of all sampling sites, Table A2 the mineralogical dataset, Table A3 the geochemical dataset, and Table A4 a summary of petrographic, heavy-mineral, and geochemical data on additional samples collected in the Niger catchment across Nigeria. The Google-Earth™ map of sampling sites NigerBudget.kmz is also provided.

DATA AVAILABILITY

The mineralogical, geochemical, and geochronological datasets from this study are available from the senior author upon request.

DECLARATION OF COMPETING INTEREST

The authors declare that they have no known competing financial interests or personal relationships that could have appeared to influence the work reported in this article.

FIGURE AND TABLE CAPTIONS

Figure 1. The Niger River in Nigeria (base map from Google Earth^{TM}) with sampling locations (more information in Appendix Table A1 and file *NigerBudget.kmz*).

Figure 2. Geomorphology of Nigeria. **A**) Annual rainfall (from Onafeso 2023); **B**) Topography (from Tijani 2023); **C**) Climatic zones (from Mobolade and Pourvahidi 2020).

Figure 3. Geological map of Nigeria (from Thiéblemont et al. 2016).

Figure 4. Very similar grain-size distribution obtained by wet sieving of Middle Niger, Benue, and Lower Niger sediment samples collected near Lokoja city. All three samples resulted to be pentamodal mixtures of clay (dispersed through the water column during fluvial transport), cohesive and frictional silt (carried as shallow and deep suspended load), very fine to fine sand (carried partly in suspension), and coarse sand (entrained as bedload; Rouse 1937; Vanoni 2006).

Figure 5. The coarse tail of the size distribution (**A**, **B**, **C**; 0.5-2 mm class) consists mostly of quartz commonly showing etch pits (Q), weathered K-feldspar (O, orthoclase; M, microcline), laterite clasts with hematite-stained matrix (h), and rare plagioclase (P) and mica (m). The coarsest tail (> 2 mm) contains clasts of pedogenic duricrusts (**D**, **E** and **F**) and rock fragments (**G**, **H**, and **I**). Blue bar for scale is 200 μm.

Figure 6. Size-dependent intrasample variability of tectosilicate proportions (Q, quartz; P, plagioclase, K, K-feldspar). **A**) In all three samples, quartz notably increases in the coarse tail of the size distribution. Very coarse size of microcline grains in parent rocks (Fig. 5G) explains why Q/F and P/F ratios − represented in **B** and **C** as moving averages between adjacent classes – drop in the coarsest tail. Sand compositional fields after Garzanti (2019; pFQ, kFQ and qFQ: P-rich, K-rich, and Q-rich feldspatho-quartzose; Q, quartzose; pQ, pure quartzose).

Figure 7. Settling-equivalence analysis (Garzanti et al. 2008). Because samples are a mixture of different size modes and quartz increases with grain size, coefficients of determination (R^2) are low and size-density curves are shifted upward by 0.2-0.5 phi units (coloured arrows) relative to theoretical size-density curves for *fSi*, *cSi*, *VFS*, and *CS* modes (calculated with Cheng's 1997 formula; coloured diamonds). ZTR minerals and anatase are much finer than expected independently of their density, pointing to recycling of fine-grained siliciclastic units. **Inset**: transparent heavy-

mineral concentration (tHMC; curves represented as moving averages) reaches maximum in the 15-63 µm range, which includes the fine tail of *fSi*, *cSi*, and *VFS* modes. Q, quartz, K, K-feldspar; P, plagioclase; a, anatase; e, epidote; g, garnet; h, hornblende; i, titanite, m, monazite, r, rutile; s, staurolite; t, tourmaline; z, zircon.

Figure 8. Intrasample geochemical variability (finest mud is < 5 µm fraction). **A**) Mg and Sc concentrate in phyllosilicate-rich clay, Zr, Hf and Lu in zircon-rich silt, and Ca, Sr and Ba in tectosilicate-rich sand where ε_{Nd} is most negative. **B**) Zircon controlling much of the Zr, Hf and Lu budgets is concentrated in silt and depleted in clay and coarse sand. Monazite and xenotime controlling much of the Th-LREE and Y-HREE budgets, respectively, also occur in the fine tail of the *CS* mode of Niger sand (180-355 µm classes; Table 1).

Figure 9. Intrasample variability of REE patterns normalized to CI carbonaceous chondrites (Barrat et al. 2012). Arrows indicate the effect of decreasing quartz and increasing monazite, xenotime, or zircon. REE are enriched in the fine tail of the size distribution where densest minerals are concentrated, and diluted in the coarse tail where quartz is most abundant. Coarse monazite and xenotime grains occur in the fine tail of the *CS* mode of Niger sand (180-355 classes; Table 1 and Fig. 8B).

Figure 10. Size-dependent intersample variability of tectosilicate proportions (Q, quartz; P, plagioclase; K, K-feldspar; data provided in Appendix Table A4). In fluvial samples collected across Nigeria, quartz systematically increases relatively to K-feldspar and K-feldspar relative to plagioclase from very fine to coarse sand. Intersample trends, sharpest for Middle Niger sand (correlation coefficients +0.92 for Q/F and -0.88 for P/F), are consistent with intrasample trends displayed by the three Lokoja samples (Fig. 6).

Figure 11. Channel profiles of the Niger and Benue rivers and their Nigerian tributaries. Steepness indices are invariably low (K_{sn} < 50), reflecting low erosive power. Channel concavity θ and normalized steepness K_{sn} are defined by a power-law relationship between the local channel slope S and the contributing drainage area A used as a proxy for discharge ($S = KsA^{-\theta}$; Flint 1974). Anomalous θ values (< 0 or > 1) are associated with knickpoints, in turn related to dams, changes in bedrock properties, differences in rock-uplift rate, or transition from incisional to depositional conditions (Whipple 2004). Further methodological details are provided in Garzanti et al. (2021b). Dams: JD, Jebba; KD, Kainji; SD, Shiroro.

Figure 12. Intrasample variability of heavy-mineral indices of recycling. ZTR peaks in silt largely because of settling-equivalence effects (i.e., marked concentration of zircon and rutile in the fine tail of *fSI* and *cSi* modes), but T/(T+Amp) also shows peaks in the same classes pointing at extensive recycling for *fSi*, *cSi* and *CS* modes (especially for Middle Niger). Consistently low indices testify to lower percentages of recycled detritus in very fine to fine sand (especially for Benue River). Z, zircon; T, tourmaline; R, rutile; Amp, amphibole). Curves for medium sand classes are dotted because of the lower number of counted tHM.

Figure 13. Multidimensional scaling map based on U-Pb zircon ages (data from Pastore et al. 2023). Benue sand contains mostly Neoproterozoic grains whereas also Paleoproterozoic zircons occur in Middle Niger sand. Distance among samples in the map reflects the dissimilarity of their chronological signatures; the "stress" value of the configuration evaluates the goodness of fit (0.1, fair; 0.05, good; Vermeesch and Garzanti 2015).

Table 1. Intrasample mineralogical variability determined by coupling optical microscopy and semi-automated Raman spectroscopy on 15 size classes of Middle Niger, Benue, and Lower Niger sediment samples. GSZ, grain size; Q, quartz; F, feldspar (P, plagioclase; K, K-feldspar); phyl, phyllosilicates (Kln, kaolinite; Sme, smectite; Ilt, illite; clay-mineral data from Bayon et al. 2024); tHMC, transparent heavy-mineral concentration; Z, zircon, T, tourmaline; R, rutile; Ti ox, anatase and brookite; Ttn, titanite; Mnz, monazite; Xtm, xenotime; Ep, epidote; Grt, garnet; St, staurolite; And, andalusite; Ky, kyanite; Sil, sillimanite; Amp, amphibole; Px, pyroxene; &tHM includes apatite, olivine, Cr-spinel, corundum, topaz, barite, vesuvianite, dumortierite, and astrophyllite; p, present; c, common, C, very common; n.d., not determined.

Table 2. Intrasample geochemical variability determined on 14 size classes of Middle Niger, Benue, and Lower Niger sediment samples.

Table 3. Summary of provenance budgets based on different approaches. All methods indicate that the Benue River supplies at least two-thirds of the sediment presently reaching the Niger Delta. Gauged fluxes after NEDECO (1961). Grain-size modes: *clay* > 9ϕ, *fSi* 9ϕ to 5ϕ, *cSi* 5ϕ to 4ϕ, *VFS* 4ϕ to 2.5ϕ, *CS* < 2ϕ; *cohesive mud* > 6ϕ, *sand* < 4ϕ.

REFERENCES

Abam, T.K.S., 1999, Impact of dams on the hydrology of the Niger Delta: Bulletin of Engineering Geology and the Environment, v. 57, p. 239-251.

Adegoke, O.S., Oyebamiji, A.S., Edet, J.J... Osterloff, P.L, and Ulu, O.K., 2017, Geology of the Niger Delta Basin, *in* Adegoke et al., eds., Cenozoic Foraminifera and Calcareous Nannofossil Biostratigraphy of the Niger Delta: Amsterdam, Elsevier, ch. 2, p. 25-66.

Andò, S., 2020, Gravimetric separation of heavy-minerals in sediments: Minerals, v. 10, n. 273, doi:10.3390/min10030273.

Andò, S., and Garzanti, E., 2014, Raman spectroscopy in heavy-mineral studies, *in* Scott, R.A., Smyth. H.R., Morton, A.C., Richardson, N., eds., Sediment provenance studies in hydrocarbon exploration and production: Geological Society of London, Special Publication 386, p. 395-412.

Andò, S., Vignola, P., and Garzanti, E., 2011, Raman counting: a new method to determine provenance of silt: Rendiconti Lincei, Scienze Fisiche e Naturali, v. 22, p. 327-347.

Attal, M., and Lavé, J., 2009, Pebble abrasion during fluvial transport: Experimental results and implications for the evolution of the sediment load along rivers: Journal of Geophysical Research: Earth Surface, v. 114, F04023, doi:10.1029/2009JF001328.

Barrat, J.A., Keller, F., Amossé, J., Taylor, R.N., Nesbitt, R.W., and Hirata, T., 1996, Determination of rare earth elements in sixteen silicate reference samples by ICP-MS after Tm addition and ion exchange separation: Geostandards Newsletter, v. 20(1), p. 133-139.

Barrat, J.A., Zanda, B., Moynier, F., Bollinger, C., Liorzou, C., and Bayon, G., 2012, Geochemistry of CI chondrites: major and trace elements, and Cu and Zn isotopes: Geochimica et Cosmochimica Acta, v. 83, p. 79–92.

Basu, A., 1976, Petrology of Holocene fluvial sand derived from plutonic source rocks: implications to paleoclimatic interpretation: Journal of Sedimentary Petrology, v. 46, p. 694-709.

Basu, A., 1985, Influence of climate and relief on compositions of sands released at source areas, *in* Zuffa, G.G., ed., Provenance of arenites: Dordrecht, Reidel, NATO ASI Series C, v. 148, p. 1-18.

Bayon, G., German, C.R., Boella, R.M., Milton, J.A., Taylor, R.N., and Nesbitt, R.W., 2002, An improved method for extracting marine sediment fractions and its application to Sr and Nd isotopic analysis: Chemical Geology, v. 187, p. 179-199.

Bayon, G., Barrat, J.A., Etoubleau, J., Benoit, M., Bollinger, C., and Révillon, S., 2009, Determination of rare earth elements, Sc, Y, Zr, Ba, Hf and Th in geological samples by ICP-MS after Tm addition and alkaline fusion: Geostandards and Geoanalytical Research, v. 33(1), p. 51-62.

Bayon, G., Garzanti, E., Dinis, P., Daniel Beaufort, D., Barrat, J.A., Germain, Y., Trinquier, A., Barbarano, M., Overare, B., and Braquet, N., 2024, Influence of Saharan dust on chemical weathering and associated phosphate release in West Africa: Earth and Planetary Science Letters, accepted pending minor revision, 19.5.2024.

Bea, F., Montero, P., and Ortega, M., 2006, A LA–ICP–MS evaluation of Zr reservoirs in common crustal rocks: implications for Zr and Hf geochemistry, and zircon-forming processes: The Canadian Mineralogist, v. 44(3), p. 693-714.

Bea, F., Montero, P., Molina, J.F., Scarrow, J.H., Cambeses, A., and Moreno, J.A., 2018, Lu-Hf ratios of crustal rocks and their bearing on zircon Hf isotope model ages: the effects of accessories: Chemical Geology, v. 484, p. 179-190.

Blatt, H., 1967a, Provenance determinations and recycling of sediments: Journal of Sedimentary Petrology, v. 37, p. 1031-1044.

Blatt, H., 1967b, Original characteristics of clastic quartz grains: Journal of Sedimentary Petrology, v. 37(2), p. 401-424.

Blatt, H., 1970, Determination of mean sediment thickness in the crust: a sedimentologic method: Geological Society of America Bulletin, v. 81(1), p. 255-262.

Blatt, H., 1985, Provenance studies and mudrocks: Journal of Sedimentary Petrology, v. 55(1), p. 69-75.

Blatt, H., and Jones, R.L., 1975, Proportions of exposed igneous, metamorphic, and sedimentary rocks: Geological Society of America Bulletin, v. 86(8), p. 1085-1088.

Bouvier, A., Vervoort, J.D., and Patchett, P.J., 2008, The Lu-Hf and Sm-Nd isotopic composition of CHUR: Constraints from unequilibrated chondrites and implications for the bulk composition of terrestrial planets: Earth and Planetary Science Letters, v. 273, p. 48-57.

Breyer, J.A., and Bart, H.A., 1978, The composition of fluvial sands in a temperate semiarid region: Journal of Sedimentary Petrology, v. 48, p. 1311-1320.

Bristow, C.S., Drake, N., and Armitage, S., 2009, Deflation in the dustiest place on Earth: the Bodélé Depression, Chad: Geomorphology, v. 105(1-2), p. 50-58.

Caquineau, S., Gaudichet, A., Gomes, L., and Legrand, M., 2002, Mineralogy of Saharan dust transported over northwestern tropical Atlantic Ocean in relation to source regions: Journal of Geophysical Research: Atmospheres, v. 107(D15), n. 4251, doi:10.1029/2000JD000247, 14 p.

Černý, P., Ercit, T.S., Smeds, S.A., Groat, L.A., and Chapman, R., 2007, Zirconium and hafnium in minerals of the columbite and wodginite groups from granitic pegmatites: The Canadian Mineralogist, v. 45(2), p. 185-202.

Chardon, D., Grimaud, J.L., Rouby, D., Beauvais, A., and Christophoul, F., 2016, Stabilization of large drainage basins over geological time scales: Cenozoic West Africa, hot spot swell growth, and the Niger River: Geochemistry, Geophysics, Geosystems, v. 17, p. 1164–1181, doi:10.1002/2015GC006169.

Charles, R.G., and Blatt, H., 1978, Quartz, chert, and feldspars in modern fluvial muds and sands: Journal of Sedimentary Petrology, v. 48(2), p. 427-432.

Cheng, N.S., 1997, Simplified settling velocity formula for sediment particle: Journal of Hydraulic Engineering, v. 123(2), p. 149-152.

Claquin, T., Schulz, M., and Balkanski, Y.J., 1999, Modeling the mineralogy of atmospheric dust sources: Journal of Geophysical Research: Atmospheres, v. 104(D18), p. 22243-22256.

Daramola, J., Adepehin, E.J., Ekhwan, T.M., Choy, L.K., Mokhtar, J., and Tabiti, T.S., 2022, Impacts of land-use change, associated land-use area and runoff on watershed sediment yield: Implications from the Kaduna watershed: Water, v. 14(3), p. 325.

Deckers, S., Dondeyne, S., Vandekerckhoven, L., and Raes, D., 1995, Major soils and their formation in the West-African Sahel, *in* Miézan, K.M., Wopereis, M.C.S., Dingkuhn, M., Deckers J., and Randokph, T.R., eds., Irrigated rice in the Sahel: Prospects for sustainable development. West Africa Rice Development Association, WARDA/ADRAO, Saint Louis, Senegal, p. 23-35.

Dott, R.H., 2003, The importance of eolian abrasion in supermature quartz sandstones and the paradox of weathering on vegetation-free landscapes: The Journal of Geology, v. 111, p. 387-405.

Drake, N.A., Candy, I., Breeze, P., Armitage, S.J., Gasmi, N., Schwenninger, J.L., Peat, D., and Manning, K., 2022, Sedimentary and geomorphic evidence of Saharan megalakes: A synthesis: Quaternary Science Reviews, v. 276, n. 107318.

Eludoyin, O.M., and Adelekan, I.O., 2013, The physiologic climate of Nigeria: International Journal of Biometeorology, v. 57(2), p. 241-264.

FAO, 1997, The Niger River basin, *in* Frenken, K., and Faurès, J.M., eds., Irrigation potential in Africa: A basin approach: Rome, Food and Agriculture Organization of the United Nations, Land and Water Bulletin, v. 4, p. 47-53, http://www.fao.org/docrep/w4347e/w4347e0i.htm

FAO, and IHE Delft, 2020, Water Accounting in the Niger River Basin: Rome, FAO WaPOR water accounting reports, 120 p., https://doi.org/10.4060/cb1274en

Feil, S., von Eynatten, H., Dunkl, I., Schönig, J., and Lünsdorf, N.K., 2024, Inherited grain-size distributions: Effect on heavy-mineral assemblages in modern and ancient sediments: Journal of Geophysical Research: Earth Surface, v. 129, e2023JF007356.

Feniak, M.W., 1944, Grain sizes and shapes of various minerals in igneous rocks: American Mineralogist: Journal of Earth and Planetary Materials, v. 29(11-12), p. 415-421.

Ferré, E., Gleizes, G., and Caby, R., 2002, Obliquely convergent tectonics and granite emplacement in the Trans-Saharan belt of Eastern Nigeria: a synthesis: Precambrian Research, v. 114(3-4), p. 199-219.

Flint, J.J., 1974, Stream gradient as a function of order, magnitude, and discharge: Water Resources Research, v. 10, p. 969–973.

Folk, R.L., 1980, Petrology of Sedimentary Rocks. Austin (USA), Hemphill Publishing Co., 184 p.

Freeman, J.J., Wang, A., Kuebler, K.E., Jolliff, B.L., and Haskin, L.A., 2008, Characterization of natural feldspars by Raman spectroscopy for future planetary exploration: The Canadian Mineralogist, v. 46(6), p. 1477-1500.

Funtua, I.I., and Elegba, S.B., 2005, Radiation exposure from high-level radiation area and related mining and processing activities of Jos Plateau, central Nigeria. Elsevier, International Congress Series, v. 1276, p. 401-402, doi:10.1016/j.ics.2004.10.006.

Gallez, A., Juo, A.S.R., Herbillon, A.J., and Moormann, F.R., 1975, Clay mineralogy of selected soils in southern Nigeria: Soil Science Society of America Journal, v. 39(3), p. 577-585.

Garzanti, E., 1986, Source rock versus sedimentary control on the mineralogy of deltaic volcanic arenites (Upper Triassic, northern Italy): Journal of Sedimentary Petrology, v. 56(2), p. 267-275.

Garzanti, E., 2017, The maturity myth in sedimentology and provenance analysis: Journal of Sedimentary Research, v. 87, p. 353-365.

Garzanti, E., 2019, Petrographic classification of sand and sandstone: Earth-Science Reviews, v. 192, p. 545-563.

Garzanti, E., and Andò, S. 2007, Heavy-mineral concentration in modern sands: implications for provenance interpretation, *in* Mange, M., and Wright, D., eds., Heavy minerals in use: Amsterdam, Elsevier, Developments in Sedimentology Series v. 58, p. 517-545.

Garzanti, E., and Andò, S., 2019, Heavy Minerals for Junior Woodchucks: Minerals, v. 9(3), n. 148, doi:10.3390/min9030148.

Garzanti, E., and Resentini, A., 2016, Provenance control on chemical indices of weathering (Taiwan river sands): Sedimentary Geology, v. 336, p. 81-95.

Garzanti, E., Andò, S., and Vezzoli, G., 2008, Settling-equivalence of detrital minerals and grain-size dependence of sediment composition: Earth and Planetary Science Letters, v. 273, p. 138–151.

Garzanti, E., Andò, S., and Vezzoli, G., 2009, Grain-size dependence of sediment composition and environmental bias in provenance studies: Earth and Planetary Science Letters, v. 277, p. 422–432.

Garzanti, E., Andò, S., France-Lanord, C., Vezzoli, G., Galy, V., and Najman, Y., 2010, Mineralogical and chemical variability of fluvial sediments. 1. Bedload sand (Ganga-Brahmaputra, Bangladesh): Earth and Planetary Science Letters, v. 299, p. 368-381.

Garzanti, E., Andò, S., France-Lanord, C., Galy, V., Censi, P., and Vignola, P., 2011, Mineralogical and chemical variability of fluvial sediments. 2. Suspended-load silt (Ganga-Brahmaputra, Bangladesh): Earth and Planetary Science Letters, v. 302, p. 107-120.

Garzanti, E., Andò, S., Vezzoli, G., Lustrino, M., Boni, M., and Vermeesch, P., 2012a, Petrology of the Namib Sand Sea: Long-distance transport and compositional variability in the wind-displaced Orange Delta: Earth-Science Reviews, v. 112(3-4), p. 173-189.

Garzanti, E., Resentini, A., Vezzoli, G., Andò, S., Malusà, M., and Padoan, M., 2012b, Forward compositional modelling of Alpine orogenic sediments: Sedimentary Geology, v. 280, p. 149-164.

Garzanti, E., Vermeesch, P., Padoan, M., Resentini, A., Vezzoli, G., and Andò, S., 2014a, Provenance of passive-margin sand (Southern Africa): The Journal of Geology, v. 122, p. 17-42.

Garzanti, E., Vermeesch, P., Andò, S., Lustrino, M., Padoan, M., and Vezzoli, G., 2014b, Ultra-long distance littoral transport of Orange sand and provenance of the Skeleton Coast Erg (Namibia): Marine Geology, v. 357, p. 25-36.

Garzanti, E., Andò, S., Padoan, M., Vezzoli, G., and El Kammar, A., 2015a, The modern Nile sediment system: Processes and products: Quaternary Science Reviews, v. 130, p. 9-56.

Garzanti, E., Resentini, A., Andò, S., Vezzoli, G., Pereira, A., and Vermeesch, P., 2015b, Physical controls on sand composition and relative durability of detrital minerals during ultra-long distance littoral and aeolian transport (Namibia and southern Angola): Sedimentology, v. 62(4), p. 971-996.

Garzanti, E., Dinis, P., Vermeesch, P., Andò, S., Hahn, A., Huvi, J., Limonta, M., Padoan, M., Resentini, A., Rittner, M., and Vezzoli, G., 2018, Dynamic uplift, recycling, and climate control on the petrology of passive-margin sand (Angola): Sedimentary Geology, v. 375, p. 86-104.

Garzanti, E., Vermeesch, P., Vezzoli, G., Andò, S., Botti, E., Limonta, M., Dinis, P., Hahn, A., Baudet, D., De Grave, J., and Yaya, N.K., 2020, Congo River sand and the equatorial quartz factory: Earth-Science Reviews, v. 197, n. 102918, doi.org/10.1016/j.earscirev.2019.102918

Garzanti, E., Bayon, G., Dennielou, B., Barbarano, M., Limonta, M., and Vezzoli, G., 2021a, The Congo deep-sea fan: Mineralogical, REE, and Nd-isotope variability in quartzose passive-margin sand: Journal of Sedimentary Research, v. 91(5), p. 433-450.

Garzanti, E., Pastore, G., Resentini, A., Vezzoli, G., Vermeesch, P., Ncube, L., Van Niekerk, H-G., Jouet, G., and Dall'Asta, M., 2021b, The segmented Zambezi sedimentary system from source to sink 1. Sand petrology and heavy minerals: The Journal of Geology, v. 129(4), p. 343-369.

Garzanti, E., Bayon, G., Vermeesch, P., Barbarano, M., Pastore, G., Resentini, A., Dennielou, B., and Jouet, G., 2022a, The Zambezi deep-sea fan: mineralogical, REE, Zr/Hf, Nd-isotope, and zircon-age variability in feldspar-rich passive-margin turbidites: Journal of Sedimentary Research, v. 92(11), p. 1022-1043.

Garzanti, E., Bayon, G., Dinis, P., Vermeesch, P., Pastore, G., Resentini, A., Barbarano, M., Ncube, L., and Van Niekerk, H.J., 2022b, The segmented Zambezi sedimentary system from source to sink: 2. Geochemistry, clay minerals, and detrital geochronology: The Journal of Geology, v. 130(3), p. 171-208.

Garzanti, E., Pastore, G., Bayon, G., Vermeesch, P., Barbarano, M., Vezzoli, G., Dinis, P., Braquet, N., and Overare, B., 2024, Petrology and geochemistry of Niger River sediments. Forthcoming.

Gbadegesin, A., Adesina, F., Orimoogunje, O., and Oderinde, F., 2023, Vegetation and Human Impact, *in* Faniran, A., Jeje, L.K., Fashae, O.A., and Olusola, A.O., eds., Landscapes and Landforms of Nigeria: Cham, Springer, p. 39-52.

Gherboudj, I., Beegum, S.N., and Ghedira, H., 2017, Identifying natural dust source regions over the Middle-East and North-Africa: Estimation of dust emission potential: Earth-Science Reviews, v. 165, p. 342-355.

Götze, J., and Lewis, R., 1994, Distribution of REE and trace elements in size and mineral fractions of high-purity quartz sands: Chemical Geology, v. 114(1-2), p. 43-57.

Götze, J., Pan, Y., and Müller, A., 2021, Mineralogy and mineral chemistry of quartz: A review: Mineralogical Magazine, v. 85(5), p. 639-664.

Graham, W.A.P., 1930, A textural and petrographic study of the Cambrian sandstones of Minnesota: The Journal of Geology, v. 38, p. 696–716.

Grimaud, J.L., Rouby, D., Chardon, D., and Beauvais, A., 2018, Cenozoic sediment budget of West Africa and the Niger delta: Basin Research, v. 30(2), p. 169-186.

Hay, W.W., 1998, Detrital sediment fluxes from continents to oceans: Chemical Geology, v. 145(3-4), p. 287-323.

Hayes, J.R., 1962, Quartz and feldspar content in South Platte, Platte, and Missouri River sands: Journal of Sedimentary Petrology, v. 32, p. 793–800.

Hospers, J., 1965, Gravity field and structure of the Niger Delta, Nigeria, West Africa: Geological Society of America Bulletin, v. 76(4), p. 407-422.

Hubert, J.F., 1962, A zircon–tourmaline–rutile maturity index and the interdependence of the composition of heavy mineral assemblages with the gross composition and texture of sandstones: Journal of Sedimentary Petrology, v. 32, p. 440-450.

Ibbeken, H., and Schleyer, R., 1991, Source and Sediment: Berlin, Springer, 283 p.

Ibe, C.U., 2020, Geochemistry of the Precambrian Basement of the Bamenda massif of southeastern Nigeria: Petrogenesis and tectonic setting: Geologica Acta, v.18-19, doi:10.1344/GeologicaActa2020.18.19

Jefford, G., 1962, Xenotime from Rayfield, Northern Nigeria: American Mineralogist: Journal of Earth and Planetary Materials, v. 47(11-12), p. 1467-1473.

Johnsson, M.J., 1993, The system controlling the composition of clastic sediments, *in* Johnsson, M.J., and Basu, A., eds., Processes Controlling the Composition of Clastic Sediments: Geological Society of America, Special Paper 284, p. 1–19.

Kelling, G., Sheng, H., and Stanley, D.J., 1975, Mineralogic composition of sand-sized sediment on the outer margin off the mid-Atlantic States: assessment of the influence of the ancestral Hudson and other fluvial systems: Geological Society of America Bulletin, v. 86(6), p. 853-862.

Kodama, Y., 1994, Downstream changes in the lithology and grain size of fluvial gravels, the Watarase River, Japan; evidence of the role of abrasion in downstream fining: Journal of Sedimentary Research, v. 64(1), p. 68-75.

Krippner, A., Meinhold, G., Morton, A.C., Russell, E., and von Eynatten, H., 2015, Grain-size dependence of garnet composition revealed by provenance signatures of modern stream sediments from the western Hohe Tauern (Austria): Sedimentary Geology, v. 321, p. 25-38.

Krippner, A., Meinhold, G., Morton, A.C., Schönig, J., and von Eynatten, H., 2016, Heavy minerals and garnet geochemistry of stream sediments and bedrocks from the Almklovdalen area, Western Gneiss Region, SW Norway: Implications for provenance analysis: Sedimentary Geology, v. 336, p. 96-105.

Kuenen, P.H., 1956, Experimental abrasion of pebbles: 2. Rolling by current: The Journal of Geology, v. 64(4), p. 336-368.

Kuenen, P.H., 1959, Experimental abrasion; 3, Fluviatile action on sand: American Journal of Science, v. 257, p. 172-190.

Lünsdorf, N.K., Kalies, J., Ahlers, P., Dunkl, I., and Von Eynatten, H., 2019, Semiautomated heavy-mineral analysis by Raman spectroscopy: Minerals, v. 9, n. 385.

McIntyre, D.D., 1959, The hydraulic equivalence and size distributions of some mineral grains from a beach: The Journal of Geology, v. 67(3), p. 278-301.

Melcher, F., Graupner, T., Gäbler, H.E., Sitnikova, M., Henjes-Kunst, F., Oberthür, T., Gerdes, A., and Dewaele, S., 2015, Tantalum–(niobium–tin) mineralisation in African pegmatites and rare metal granites: Constraints from Ta–Nb oxide mineralogy, geochemistry and U–Pb geochronology: Ore Geology Reviews, v. 64, p. 667-719.

Milliman, J.D., and Farnsworth, K.L. 2011, River discharge to the coastal ocean: a global synthesis. Cambridge (UK), Cambridge University Press, 384 p.

Møberg, J.P., and Esu, I.E., 1991, Characteristics and composition of some savanna soils in Nigeria: Geoderma, v. 48(1-2), p. 113-129.

Mobolade, D.T., and Pourvahidi, P., 2020, Bioclimatic approach for climate classification of Nigeria: Sustainability, v. 12(10), n. 4192.

Morton, A.C., and Hallsworth, C.R., 1999, Processes controlling the composition of heavy mineral assemblages in sandstones: Sedimentary Geology, v. 124(1-4), p. 3-29.

Moussa, M.B., Touré, A.A., Kergoat, L., Lartiges, B., Rochelle-Newall, E., Robert, E., Gosset, M., Tanimoun, B.A., and Grippa, M., 2022, Spatio-temporal dynamics of suspended particulate matter in the middle Niger River using in-situ and satellite radiometric measurements: Journal of Hydrology: Regional Studies, v. 41, n. 101106.

Muggler, C.C., Buurman, P., and van Doesburg, J.D., 2007, Weathering trends and parent material characteristics of polygenetic Oxisols from Minas Gerais, Brazil: I. Mineralogy: Geoderma, v. 138(1-2), p. 39-48.

NEDECO, 1961, The waters of the Niger Delta: The Hague, Netherlands Engineering Consultants, 317 p.

Nesbitt, H.W., and Young, G.M., 1982, Early Proterozoic climates and plate motions inferred from major element chemistry of lutites: Nature, v. 299, p. 715-717.

Nesbitt, H.W., and Young, G.M., 1996, Petrogenesis of sediments in the absence of chemical weathering: effects of abrasion and sorting on bulk composition and mineralogy: Sedimentology, v. 43, p. 341-358.

Nesbitt, H.W., Young, G.M., McLennan, S.M., and Keays, R.R., 1996, Effects of chemical weathering and sorting on the petrogenesis of siliciclastic sediments, with implications for provenance studies: The Journal of Geology, v. 104(5), p. 525-542.

Nesbitt, H.W., Fedo, C.M., and Young, G.M., 1997, Quartz and feldspar stability, steady and non-steady-state weathering, and petrogenesis of siliciclastic sands and muds: The Journal of Geology, v. 105, p. 173–192.

Ngako, V., Njonfang, E., Aka, F.T., Affaton, P., and Nnange, J.M., 2006, The North–South Paleozoic to Quaternary trend of alkaline magmatism from Niger–Nigeria to Cameroon: complex interaction between hotspots and Precambrian faults: Journal of African Earth Sciences, v. 45(3), p. 241-256.

Odom, A.L., and Rink, W.J., 1989, Giant radiation-induced color halos in quartz: solution to a riddle: Science, v. 246(4926), p. 107-109.

Odom, I.E., 1975, Feldspar-grain size relations in Cambrian arenites, upper Mississippi Valley: Journal of Sedimentary Petrology, v. 45(3), p. 636-650.

Odom, I.E., Doe, T.W., and Dott, R.H., 1976, Nature of feldspar-grain size relations in some quartz-rich sandstones: Journal of Sedimentary Petrology, v. 46, p. 862-870.

Ogunkoya, O.O., 2023, Kainji Dam and Lake, *in* Faniran, A., Jeje, L.K., Fashae, O.A., and Olusola, A.O., eds., Landscapes and Landforms of Nigeria: Cham, Springer, p. 161-174.

Ojo, O.J., Adepoju, S.A., Adewole, T.M., and Abiola, A.O., 2011, Sedimentological and geochemical studies of Maastrichtian clays in Bida Basin, Nigeria: Implication for resource potential: Centrepoint Journal (Science Edition), v. 17(2), p. 71-88.

Ojo, G.P., Igbokwe, U.G., Egbuachor, C.J., and Nwozor, K.K., 2017, Geotechnical properties and geochemical composition of kaolin deposits in parts of Ifon, Southwestern Nigeria: American Journal of Engineering Research, v. 6, p. 15-24.

Olayinka-Dosunmu, D.N., Adzandeh, A.E., Hamid-Mosaku, I.A., Okolie, C.J., Nwilo, P.C., and Ogbeta, C.O., 2022, Assessing River Benue flow data for flood mitigation and management in Adamawa catchment, Nigeria: Scientific African, v. 16, e01205.

Olivry, J.C., Bricquet, J.P., Bamba, F., and Diara, M., 1995, Le régime hydrologique du Niger supérieur et le déficit des deux dernières décennies, *in* Olivry, J.C., and Boulègue, J., eds., Grands Bassins Fluviaux Périatlantiques: Congo, Niger, Amazone : Paris, ORSTOM, Collection Colloque and Séminaire, p. 251– 266.

Olomoda, I.A., 2012, Challenges of continued river Niger low flow into Nigeria: Nigerian Association of Hydrological Sciences, Special Publication Hydrology for Disaster Management, p. 145-155.

Onafeso, O.D., 2023, The climate of Nigeria and its role in landscape modification, *in* Faniran, A., Jeje, L.K., Fashae, O.A., and Olusola, A.O., eds., Landscapes and Landforms of Nigeria: Cham, Springer, p. 33-38.

Otto, G.H., 1938, The sedimentation unit and its use in field sampling: The Journal of Geology, v. 46, p. 569-582.

Pastore, G., Baird, T., Vermeesch, P., Bristow, C., Resentini, A., and Garzanti, E., 2021, Provenance and recycling of Sahara Desert sand: Earth-Science Reviews, v. 216, n. 103606.

Pastore, G., Garzanti, E., Vermeesch, P., Bayon, G., Resentini, A., Braquet, N., and Overare, B., 2023. The zircon story of the Niger River: Time-structure maps of the West African Craton and discontinuous propagation of provenance signals across a disconnected sediment-routing system: Journal of Geophysical Research, Earth Surface, v. 128, e2023JF007342, https://doi.org/10.1029/2023JF007342

Reijers, T., 2011, Stratigraphy and sedimentology of the Niger Delta: Geologos, v. 17(3), p. 133-162, doi: 10.2478/v10118-011-0008-3.

Resentini, A., Goren, L., Castelltort, S., and Garzanti, E., 2017, Partitioning sediment flux by provenance and tracing erosion patterns in Taiwan: Journal of Geophysical Research: Earth Surface, v. 122(7), p. 1430-1454.

Resentini, A., Andò, S., and Garzanti, E., 2018, Quantifying roundness of detrital minerals by image analysis: sediment transport, shape effects, and provenance implications: Journal of Sedimentary Research, v. 88, p. 276–289.

Rouse, H., 1937, Modern conceptions of the mechanics of fluid turbulence: Transactions of the American Society of Civil Engineers, v. 102, paper n°1965, p. 463-543.

Rubey, W.W., 1933, The size-distribution of heavy minerals within a water-laid sandstone: Journal of Sedimentary Petrology, v. 3, p. 3–29.

Russell, R.D., 1937, Mineral composition of Mississippi River sands: Geological Society of America Bulletin, v. 48, p. 1307-1348.

Scheuvens, D., Schütz, L., Kandler, K., Ebert, M., and Weinbruch, S., 2013, Bulk composition of northern African dust and its source sediments — A compilation: Earth-Science Reviews, v. 116, p. 170-194.

Schönig, J., von Eynatten, H., Meinhold, G., and Lünsdorf, N.K., 2021, Life-cycle analysis of coesite-bearing garnet: Geological Magazine, v. 158(8), p. 1421-1440.

Shukri, N.M., 1950, The mineralogy of some Nile sediments: Quarterly Journal of the Geological Society of London, v. 105, p. 511-534.

Tanaka, T., Togashi, S., Kamioka, H., Amakawa, H., Kagami, H., Hamamoto, T., Yuhara, M., Orihashi, Y., Yoneda, S., Shimizu, H., and Kunimaru, T., 2000, JNdi-1: a neodymium isotopic reference in consistency with LaJolla neodymium: Chemical Geology, v. 168(3-4), p. 279-281.

Thiéblemont, D., Chêne, F., Liégeois, J.,P., Ouabadi, A., Le Gall, B., Maury, R.C., Jalludin, M., Ouattara Gbélé, C., Tchaméni, R., and Fernandez-Alonso, M., 2016, Geological map of Africa at 1:10 Million scale: Orléans (France), Commission for the Geological Map of the World–Bureau de Recherches Géologiques et Minières, 35th International Geology Congress CCGM-BRGM.

Tijani, M.N., 2023, Geology of Nigeria, *in* Faniran, A., Jeje, L.K., Fashae, O.A., and Olusola, A.O., eds., Landscapes and Landforms of Nigeria: Cham, Springer, p. 3-32.

Tuttle, M.L., Charpentier, R.R., and Brownfield, M.E., 1999, The Niger Delta petroleum system: Niger Delta Province, Nigeria, Cameroon, and Equatorial Guinea, Africa: US Department of the Interior, US Geological Survey, Open-File Report 99-50, 65 p.

Vanoni, V.A., 2006, Sedimentation engineering: Reston (USA), American Society of Civil Engineers, ASCE Manuals and Reports in Engineering Practice, v. 54, 418 p.

Vermeesch, P., and Garzanti, E., 2015, Making geological sense of 'Big Data' in sedimentary provenance analysis: Chemical Geology, v. 409, p. 20-27.

von Eynatten, H., and Dunkl, I., 2012, Assessing the sediment factory: The role of single grain analysis: Earth-Science Reviews, v. 115(1-2), p. 97-120.

von Eynatten, H., Tolosana-Delgado, R., and Karius, V., 2012, Sediment generation in modern glacial settings: Grain-size and source-rock control on sediment composition: Sedimentary Geology, v. 280, p. 80-92.

von Eynatten, H., Tolosana-Delgado, R., Karius, V., Bachmann, K., and Caracciolo, L., 2016, Sediment generation in humid Mediterranean setting: Grain-size and source-rock control on sediment geochemistry and mineralogy (Sila Massif, Calabria): Sedimentary Geology, v. 336, p. 68-80.

Wang, X., Griffin, W.L., and Chen, J., 2010, Hf contents and Zr/Hf ratios in granitic zircons: Geochemical Journal, v. 44(1), p. 65-72.

Welcomme, R.L., and Dumont, H.L., 1986, The Niger River system, *in* Davies, B.R., and Walker, K.F., eds., The Ecology of River Systems; Dordrecht, Springer, Monographiae Biologicae, v. 60, p. 9-59, doi.org/10.1007/978-94-017-3290-1_2

Weyer, S., Münker, C., Rehkämper, M., and Mezger, K., 2002, Determination of ultra-low Nb, Ta, Zr and Hf concentrations and the chondritic Zr/Hf and Nb/Ta ratios by isotope dilution analyses with multiple collector ICP-MS: Chemical Geology, v. 187(3-4), p. 295-313.

Whipple, K.X., 2004, Bedrock rivers and the geomorphology of active orogens: Annual Review of Earth and Planetary Sciences, v. 32, p. 151-185.

Whitmore, G.P., Crook, K.A., and Johnson, D.P., 2004, Grain size control of mineralogy and geochemistry in modern river sediment, New Guinea collision, Papua New Guinea: Sedimentary Geology, v. 171(1-4), p. 129-157.

Yue, H., Gebremichael, M., and Nourani, V., 2022, Performance of the Global Forecast System's medium-range precipitation forecasts in the Niger river basin using multiple satellite-based products: Hydrology and Earth System Sciences, v. 26(1), p. 167-181.

Zeese, R., 1991, Paleosols of different age in Central and Northeast Nigeria: Journal of African Earth Sciences (and the Middle East), v. 12(1-2), p. 311-318.

Zeese, R., 1996, Tertiary weathering profiles in central Nigeria as indicators of paleoenvironmental conditions: Geomorphology, v. 16(1), p. 61-70.

Zeese, R., Schwertmann, U., Tietz, G.F., and Jux, U., 1994, Mineralogy and stratigraphy of three deep lateritic profiles of the Jos Plateau (Central Nigeria): Catena, v. 21(2-3), p. 195-214.

Sahel
Lake Chad
Niamey
Sokoto
Niger
NIGERIA
Ka
Kainji Lake
Kaduna
Shiroro Lake
Oli
Jebba Dam
Niger
Okwa
Mada
Shemanker
Benue
Dep
Lokoja
Katsina -Ala
Lagos
Gulf of Guinea
N
W
E
S
0 km 200
SAMPLES
river sand
Lokoya triplet
14°
13°
12°
11°
10°
9°
8°
7°
6°
5°
4°
11°
12°
13°
14°
15°
16°

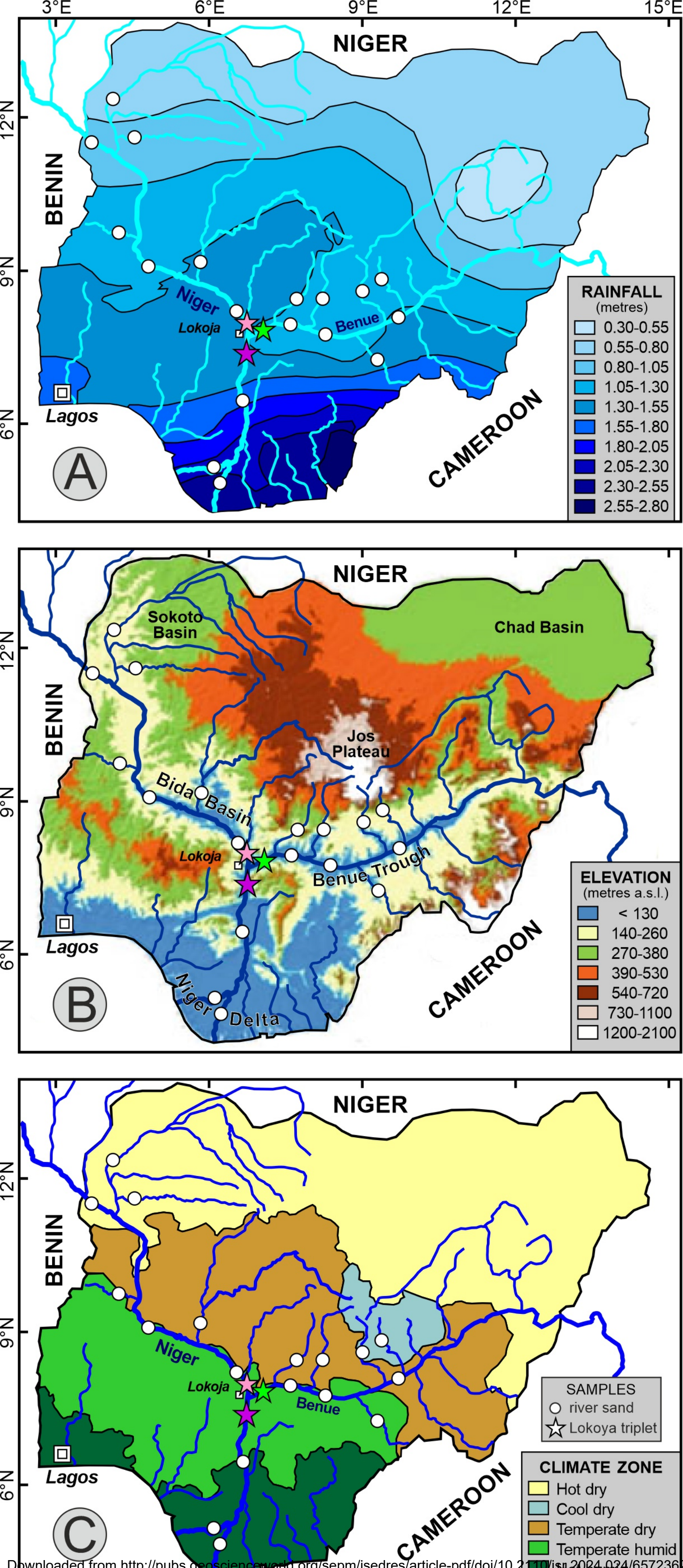

3°E
6°E
9°E
12°E
15°E
12°N
9°N
6°N
NIGER
BENIN
CAMEROON
Niger
Benue
Lokoja
Lagos
A
RAINFALL
(metres)
0.30-0.55
0.55-0.80
0.80-1.05
1.05-1.30
1.30-1.55
1.55-1.80
1.80-2.05
2.05-2.30
2.30-2.55
2.55-2.80
Sokoto Basin
Chad Basin
Jos Plateau
Bida Basin
Benue Trough
Niger Delta
B
ELEVATION
(metres a.s.l.)
< 130
140-260
270-380
390-530
540-720
730-1100
1200-2100
C
SAMPLES
river sand
Lokoya triplet
CLIMATE ZONE
Hot dry
Cool dry
Temperate dry
Temperate humid
Hot humid

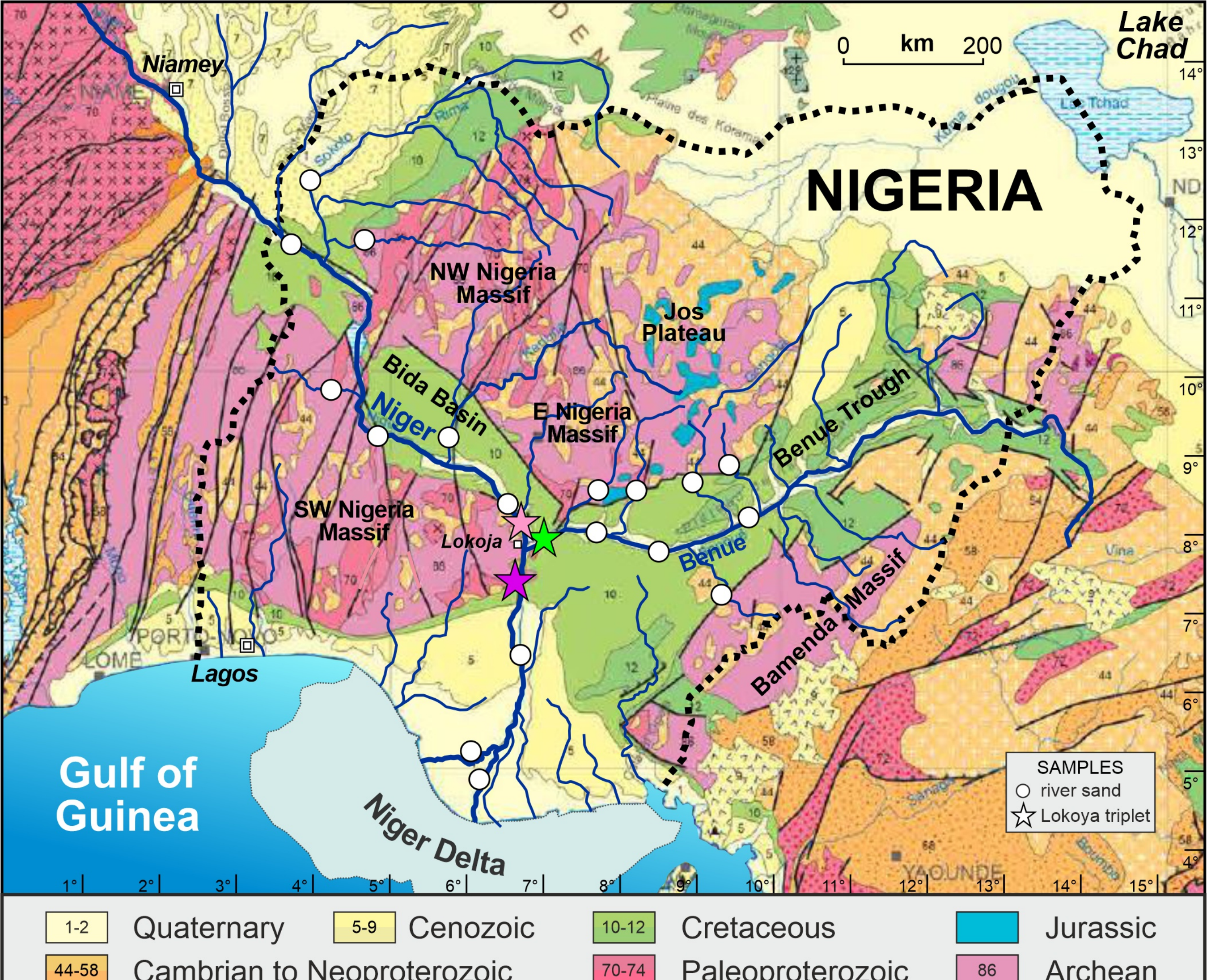
Lake Chad
0 km 200
Niamey
NIGERIA
NW Nigeria Massif
Jos Plateau
Bida Basin
Niger
E Nigeria Massif
Benue Trough
SW Nigeria Massif
Lokoja
Benue
Bamenda Massif
Lagos
Gulf of Guinea
Niger Delta
SAMPLES
river sand
Lokoya triplet
1° 2° 3° 4° 5° 6° 7° 8° 9° 10° 11° 12° 13° 14° 15°
14° 13° 12° 11° 10° 9° 8° 7° 6° 5° 4°
1-2 Quaternary
5-9 Cenozoic
10-12 Cretaceous
Jurassic
44-58 Cambrian to Neoproterozoic
70-74 Paleoproterozoic
86 Archean

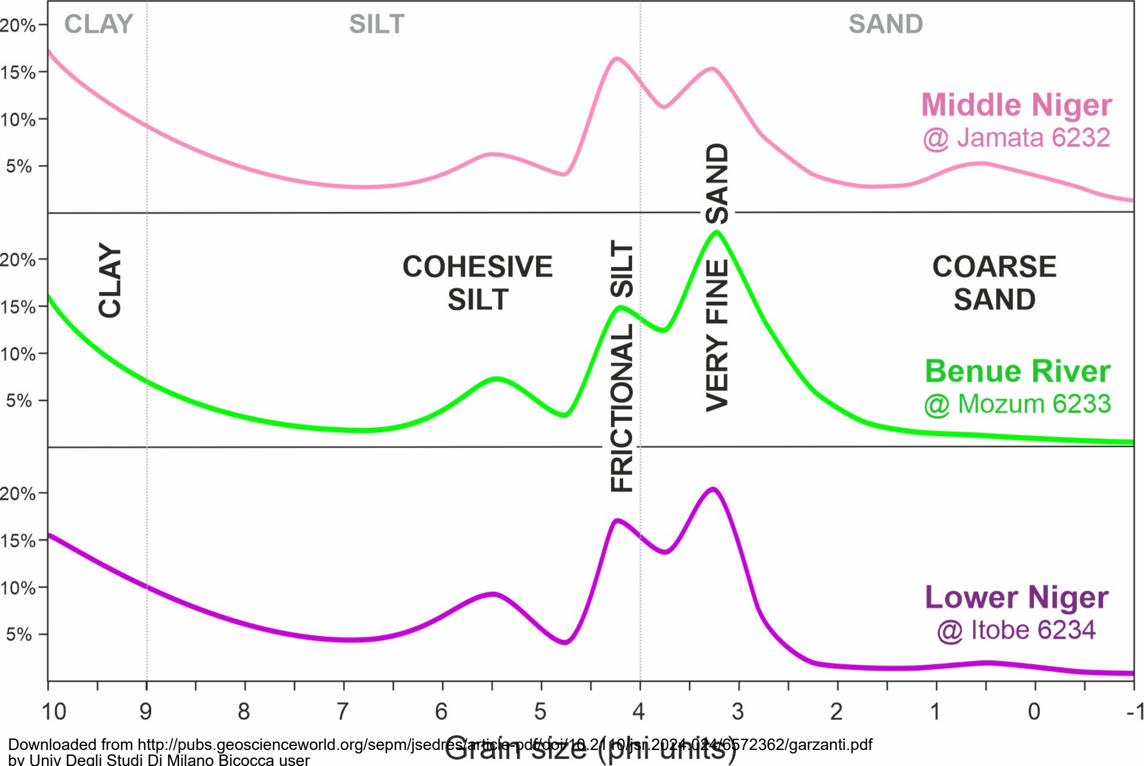

CLAY
SILT
SAND
Middle Niger
@ Jamata 6232
CLAY
COHESIVE SILT
FRICTIONAL SILT
VERY FINE SAND
COARSE SAND
Benue River
@ Mozum 6233
Lower Niger
@ Itobe 6234
20%
15%
10%
5%
10 9 8 7 6 5 4 3 2 1 0 -1
Grain size (phi units)

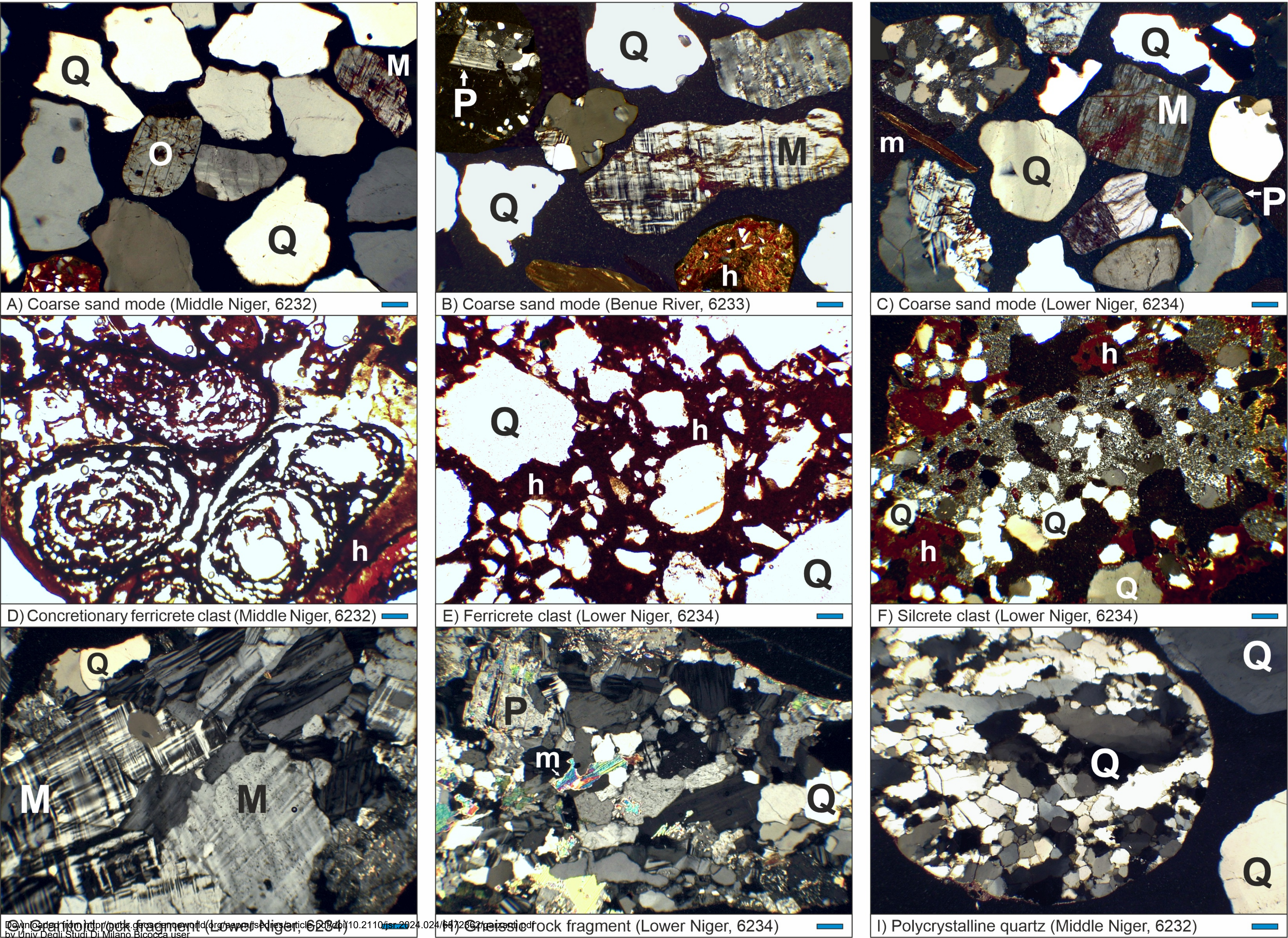

Q
M
O
Q
A) Coarse sand mode (Middle Niger, 6232)
P
Q
M
Q
h
B) Coarse sand mode (Benue River, 6233)
Q
m
M
Q
P
C) Coarse sand mode (Lower Niger, 6234)
h
D) Concretionary ferricrete clast (Middle Niger, 6232)
Q
h
h
Q
E) Ferricrete clast (Lower Niger, 6234)
h
Q
Q
h
Q
F) Silcrete clast (Lower Niger, 6234)
Q
M
M
G) Granitoid rock fragment (Lower Niger, 6234)
P
m
Q
H) Gneissic rock fragment (Lower Niger, 6234)
Q
Q
Q
I) Polycrystalline quartz (Middle Niger, 6232)

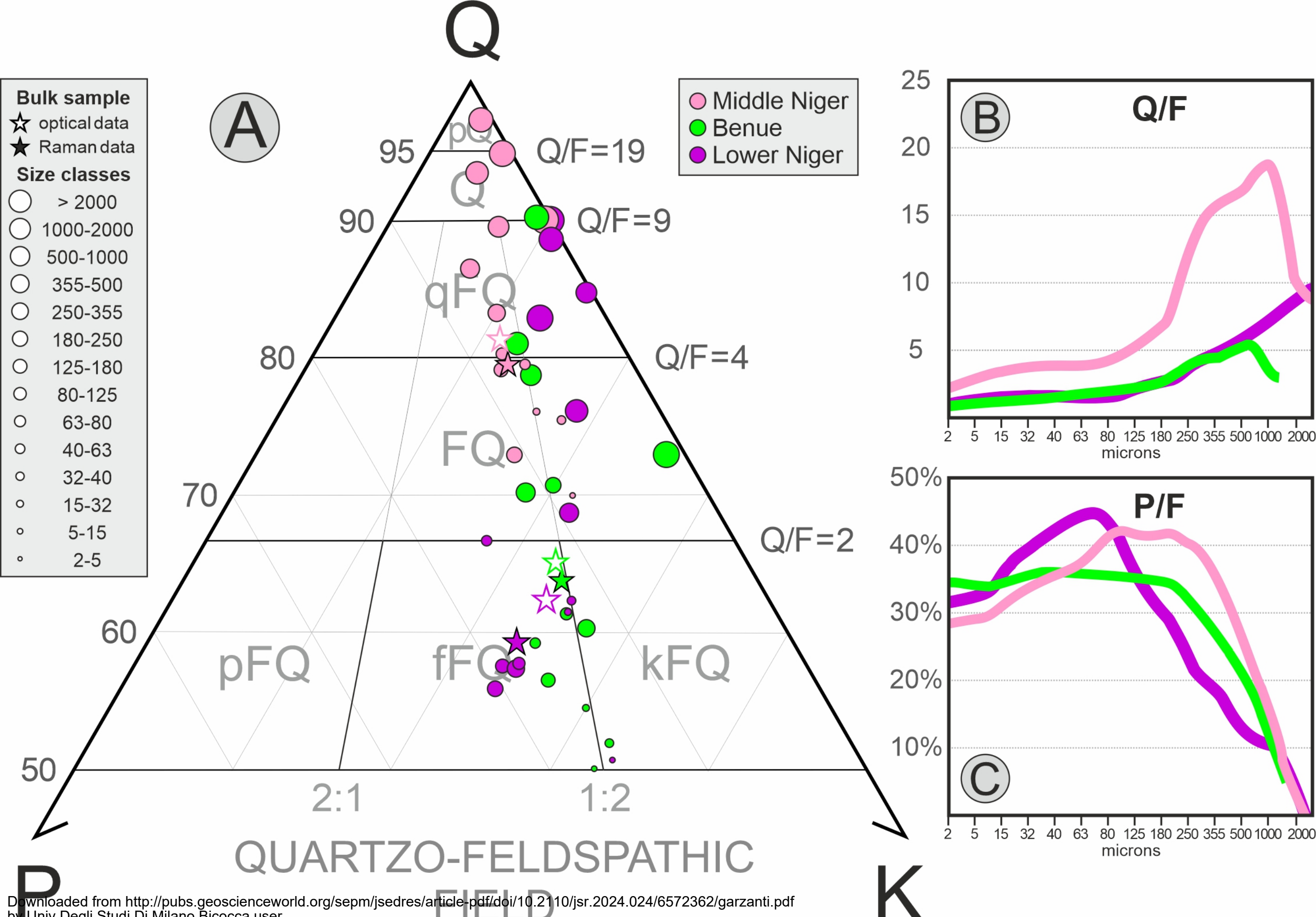
Q
P
K
A
Bulk sample
optical data
Raman data
Size classes
> 2000
1000-2000
500-1000
355-500
250-355
180-250
125-180
80-125
63-80
40-63
32-40
15-32
5-15
2-5
Middle Niger
Benue
Lower Niger
pQ
Q
qFQ
FQ
pFQ
fFQ
kFQ
95
90
80
70
60
50
Q/F=19
Q/F=9
Q/F=4
Q/F=2
2:1
1:2
QUARTZO-FELDSPATHIC FIELD
B
Q/F
25
20
15
10
5
2 5 15 32 40 63 80 125 180 250 355 500 1000 2000
microns
C
P/F
50%
40%
30%
20%
10%
2 5 15 32 40 63 80 125 180 250 355 500 1000 2000
microns

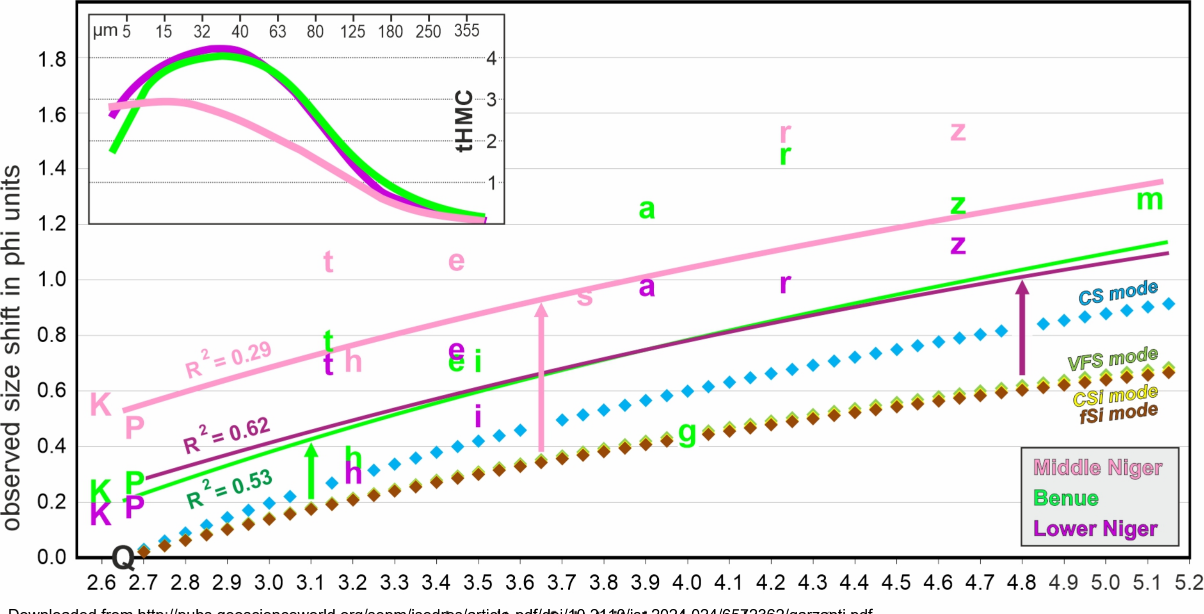
observed size shift in phi units
density of detrital minerals (g/cm³)
µm 5 15 32 40 63 80 125 180 250 355
tHMC
$R^2 = 0.29$
$R^2 = 0.62$
$R^2 = 0.53$
CS mode
VFS mode
CSi mode
fSi mode
Middle Niger
Benue
Lower Niger
Q
K
P
t
h
e
i
s
a
g
r
z
m

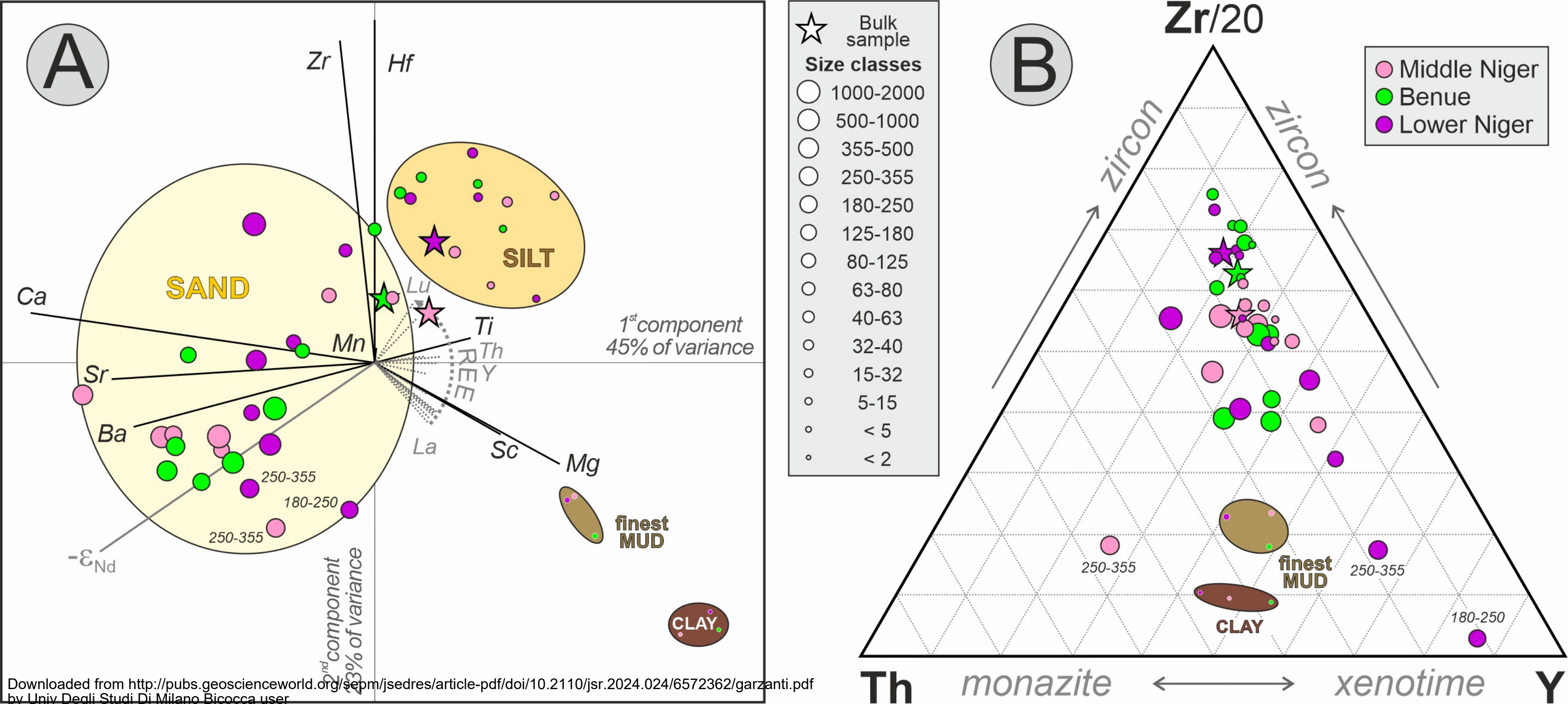
A
Zr
Hf
SILT
SAND
Ca
Mn
Lu
Ti
Th
Y
REE
La
Sr
Ba
Sc
Mg
1st component
45% of variance
2nd component
23% of variance
-εNd
250-355
180-250
250-355
finest
MUD
CLAY
Bulk sample
Size classes
1000-2000
500-1000
355-500
250-355
180-250
125-180
80-125
63-80
40-63
32-40
15-32
5-15
< 5
< 2
B
Zr/20
Middle Niger
Benue
Lower Niger
zircon
zircon
250-355
250-355
finest
MUD
CLAY
180-250
Th
monazite
xenotime
Y

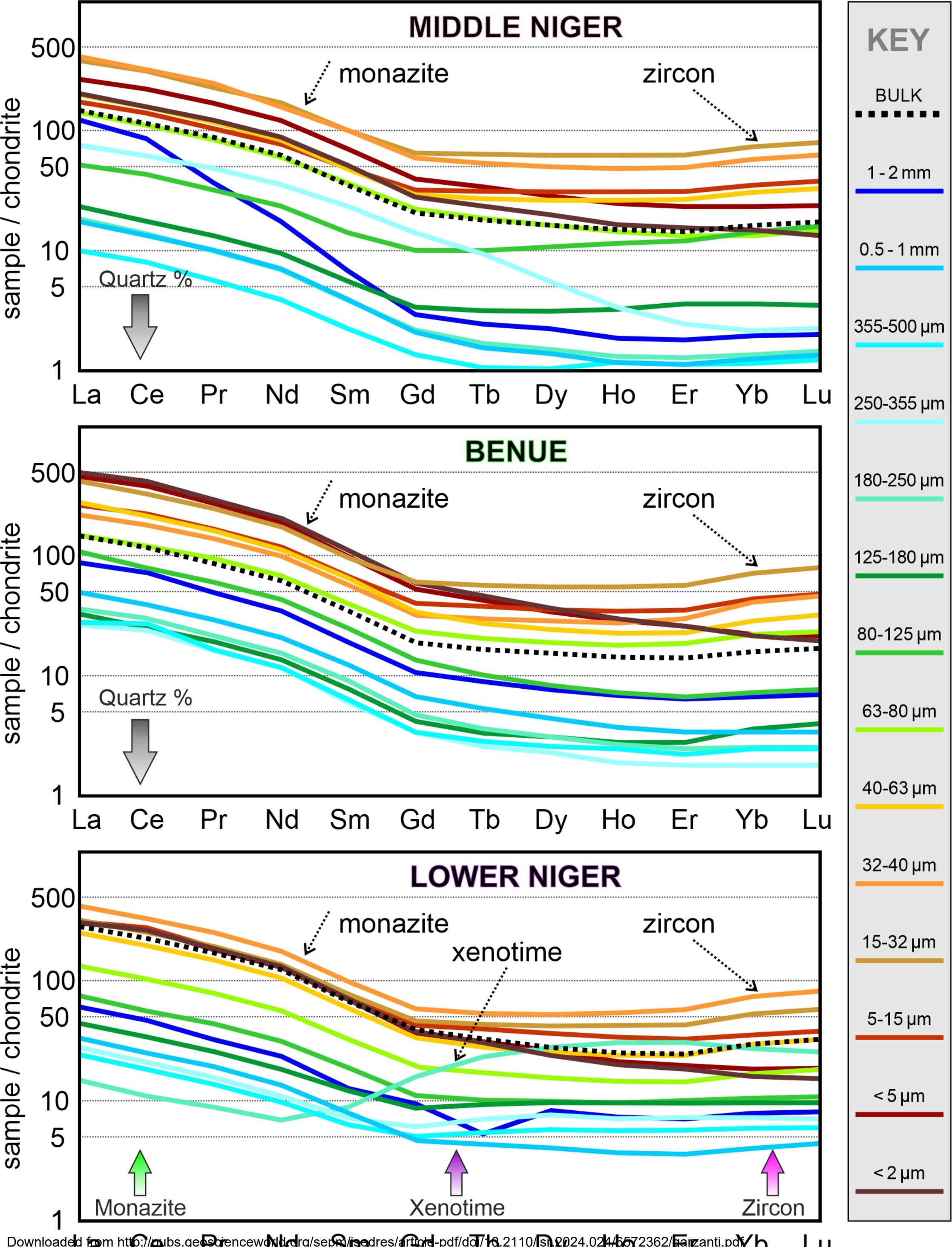
MIDDLE NIGER
monazite
zircon
Quartz %
BENUE
monazite
zircon
Quartz %
LOWER NIGER
monazite
zircon
xenotime
Monazite
Xenotime
Zircon
sample / chondrite
500
100
50
10
5
1
La
Ce
Pr
Nd
Sm
Gd
Tb
Dy
Ho
Er
Yb
Lu
KEY
BULK
1 - 2 mm
0.5 - 1 mm
355-500 µm
250-355 µm
180-250 µm
125-180 µm
80-125 µm
63-80 µm
40-63 µm
32-40 µm
15-32 µm
5-15 µm
< 5 µm
< 2 µm

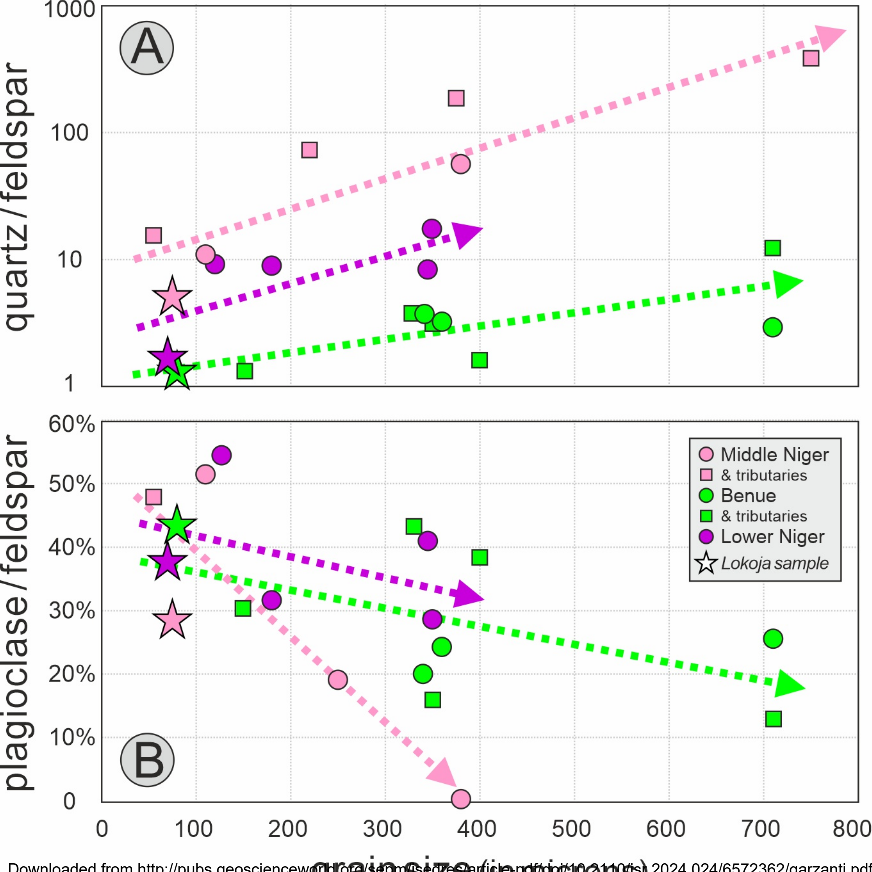
A
B
quartz / feldspar
plagioclase / feldspar
1000
100
10
1
60%
50%
40%
30%
20%
10%
0
0
100
200
300
400
500
600
700
800
grain size (in microns)
Middle Niger
& tributaries
Benue
& tributaries
Lower Niger
Lokoja sample

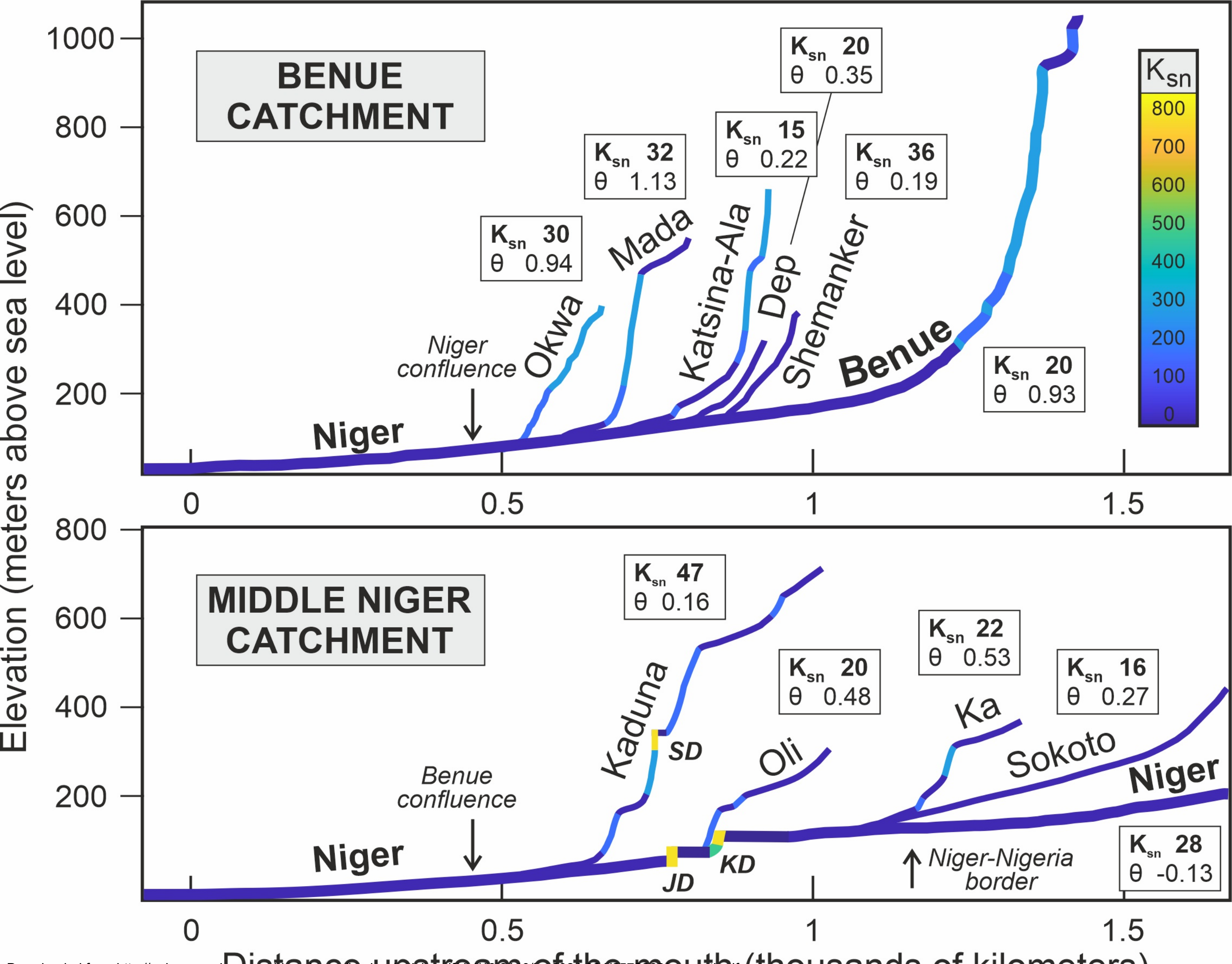
BENUE CATCHMENT
MIDDLE NIGER CATCHMENT
Elevation (meters above sea level)
Distance upstream of the mouth (thousands of kilometers)
K_{sn}
800
700
600
500
400
300
200
100
0
K_{sn} 30 θ 0.94
K_{sn} 32 θ 1.13
K_{sn} 15 θ 0.22
K_{sn} 20 θ 0.35
K_{sn} 36 θ 0.19
K_{sn} 20 θ 0.93
Niger
Niger confluence
Okwa
Mada
Katsina-Ala
Dep
Shemanker
Benue
K_{sn} 47 θ 0.16
K_{sn} 20 θ 0.48
K_{sn} 22 θ 0.53
K_{sn} 16 θ 0.27
K_{sn} 28 θ -0.13
Benue confluence
Kaduna
SD
Oli
Ka
Sokoto
JD
KD
Niger-Nigeria border

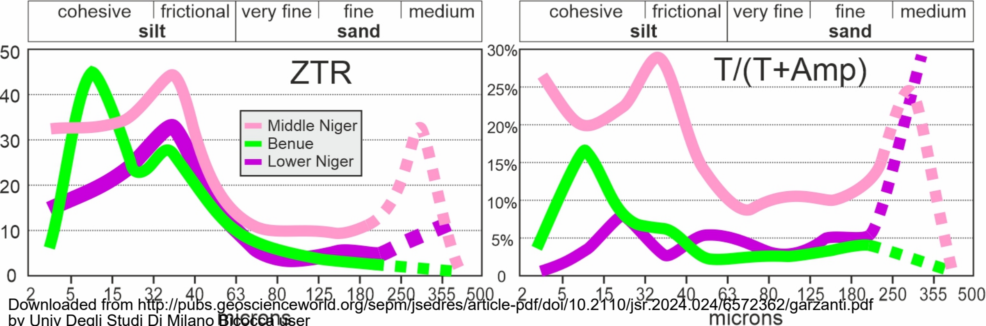

cohesive
frictional
silt
very fine
fine
medium
sand
ZTR
Middle Niger
Benue
Lower Niger
50
40
30
20
10
0
2
5
15
32
40
63
80
125
180
250
355
500
microns
T/(T+Amp)
30%
25%
20%
15%
10%
5%
0
microns

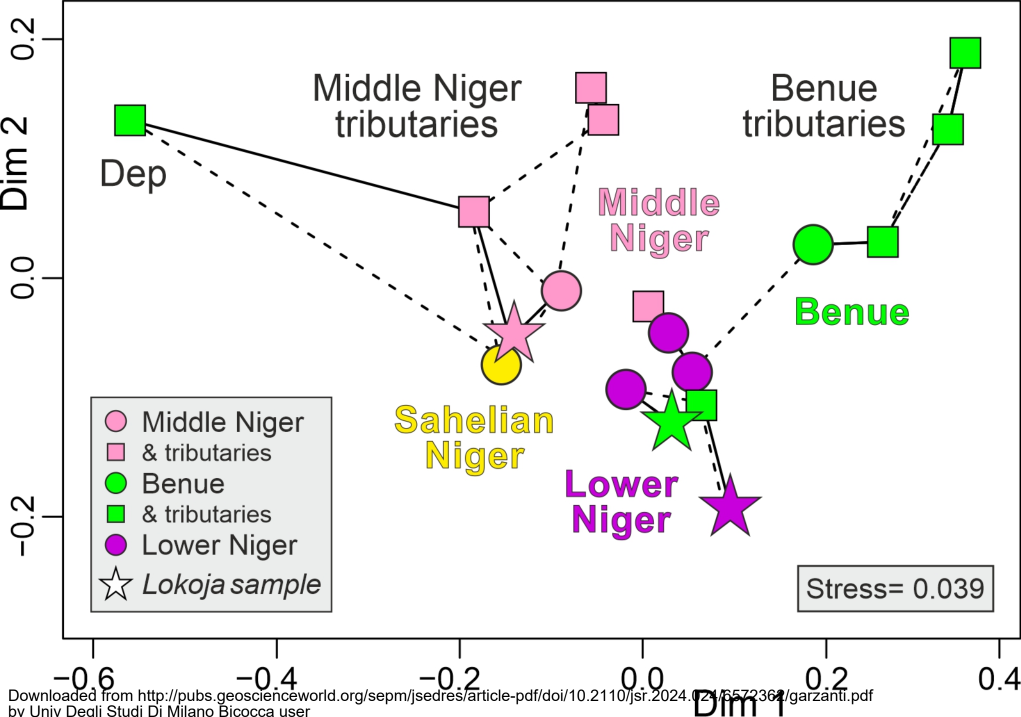

0.2
0.0
−0.2
Dim 2
−0.6
−0.4
−0.2
0.0
0.2
0.4
Dim 1
Middle Niger
tributaries
Benue
tributaries
Dep
Middle
Niger
Benue
Sahelian
Niger
Lower
Niger
Middle Niger
& tributaries
Benue
& tributaries
Lower Niger
Lokoja sample
Stress= 0.039

GSZ	class	Q	P	K	Q/F	P/F	phyl	tHMC	Z	T	R	Ti Ox	Ttn	Mnz	Xtm	Ep	Grt	St	And	Ky	Sil	Amp	Px	&tHM	Tot	ZTR	T/(T+ Amp)
μm	weight%																										
MIDDLE NIGER @ Jamata (sample 6232)																											
< 2	16%	class analyzed by XRD: **Kln**$_{69}$ **Sme**$_{18}$ **Ilt**$_{13}$												class not analyzed for heavy minerals													
2-5	2%	70	9	21	2.3	29%	7%	2.7	20	7	5	15	0.5	1.5	0.5	18	0.5	0	1	1	8	20	0.5	1	100.0	32	27%
5-15	2%	76	8	16	3.2	33%	2%	2.8	23	4	4	7	0	0.5	0	29	0	0.5	1	1	8	19	0.5	1	100.0	32	19%
15-32	6%	75	7	18	3.1	27%	1%	3.0	22	9	4	2	0.5	1.4	0	20	0	2	1	0	5	32	0	0	100.0	36	23%
32-40	4%	79	7	14	3.9	33%	0.2%	2.6	32	9	4	2	1	0.9	0.4	23	0.4	0	2	1	4	21	0	0	100.0	45	29%
40-63	17%	80	8	12	4.0	40%	0.4%	2.2	10	6	4	1	0	0	0.5	28	1	1	4	0.5	3	40	0	0	100.0	20	14%
63-80	11%	79	8	12	3.8	41%	0.3%	1.8	5	5	0.5	0	0	0.5	0	26	0.5	0.5	6	0.5	1	55	0.5	0	100.0	10	8%
80-125	15%	73	11	16	2.7	40%	0.3%	1.3	2	7	0	0	0	0.0	0	18	1	3	7	0.5	2	59	0.5	0	100.0	9	11%
125-180	8%	83	7	10	5.0	40%	0.7%	0.5	0.5	7	0.5	0.5	0	0.5	0	11	0.5	1	7	0	3	67	0.5	0	100.0	8	9%
180-250	4%	86	7	7	6.4	51%	0.2%	0.1	3	8	0.7	0	0	1	0	6	0.7	8	8	0	4	60	0.7	0	100.0	12	12%
250-355	3%	90	4	7	8.5	34%	0.8%	0.04	p	p	---	---	---	---	---	---	---	---	---	---	---	C	---	---		33	25%
355-500	3%	93	3	4	14	45%	0.2%	0.03	---	---	---	---	---	---	---	p	p	p	---	---	---	---	---	---		n.d.	n.d.
500-1000	5%	97	1	2	35	29%	0.2%					class not analyzed for insufficient amount of heavy minerals															
1000-2000	3%	95	1	4	19	13%	0%					class not analyzed for insufficient amount of heavy minerals															
> 2000	1%	90	0	10	9	0%	0%					class not analyzed for insufficient amount of heavy minerals															
BULK	100%	**79**	**7**	**13**	**6.0**	**36%**	**1.5%**	**1.5**	**14**	**7**	**3**	**5**	**0.2**	**0.7**	**0.3**	**22**	**0.7**	**1**	**3**	**0.6**	**5**	**36**	**0.3**	**0.3**	100.0	**24**	**16%**
BENUE RIVER @ Mozum (sample 6233)																											
< 2	14%	class analyzed by XRD: **Kln**$_{62}$ **Sme**$_{5}$ **Ilt**$_{33}$												class not analyzed for heavy minerals													
2-5	2%	50	17	33	1.0	35%	2%	1.7	4	1	3	23	5	1.5	0	27	0.5	0	0	0.5	2	31	2	2	100.0	8	3%
5-15	1%	55	16	30	1.2	34%	0.7%	3.4	39	4	7	2	2	1.0	0	22	0	0	0.5	0	3	17	0.5	0.5	100.0	51	19%
15-32	7%	52	15	33	1.1	32%	0.2%	5.0	16	2	3	2	3	1.4	0	28	1	0	0	0	2	39	0.5	1	100.0	22	6%
32-40	3%	59	16	24	1.5	40%	0%	4.0	22	3	3	1	4	0.5	0	32	0	0	0	0	1	33	0.5	0	100.0	28	8%
40-63	15%	61	13	25	1.6	34%	0.1%	4.2	8	0.5	1	0.5	4	0	0	27	1	0.5	0	1	0.5	54	0.5	0.5	100.0	10	1%
63-80	12%	57	17	27	1.3	39%	0.4%	3.2	3	1	1	1	3	0	0	23	0.5	0	0	0.5	0.5	64	1	0.5	100.0	5	2%
80-125	23%	71	9	20	2.4	32%	0.3%	2.5	2	1	0	0	3	0.4	0	19	1	0	0	0.4	0.4	70	3	0.4	100.0	3	1%
125-180	13%	60	13	27	1.5	32%	0.5%	0.9	0.5	2	0	0	1	0	0	15	2	1	1	0	0.5	73	2	1	100.0	2	3%
180-250	5%	70	11	18	2.3	38%	0.4%	0.4	0	2	0	0	3	0	0	22	4	1	2	0	1	62	1	0	100.0	2	4%
250-355	2%	79	7	14	3.7	33%	0%	0.2	0.7	0.7	0	0	2	0	0	24	6	0.7	2	0.7	1	60	0.7	0	100.0	1	1%
355-500	1%	81	7	12	4	35%	0%	0.2	---	---	---	---	p	---	---	c	p	---	---	---	---	C	---	p		0	0%
500-1000	1%	90	1	9	9	8%	0%					class not analyzed for insufficient amount of heavy minerals															
1000-2000	0.5%	73	1	26	3	5%	0%					class not analyzed for insufficient amount of heavy minerals															
> 2000	0.2%	Not analyzed for insufficient n° of grains										class not analyzed for insufficient amount of heavy minerals															
BULK	100%	**62**	**13**	**25**	**1.8**	**34%**	**0.5%**	**2.6**	**6**	**0.8**	**1**	**2**	**3**	**0.3**	**0**	**20**	**2**	**0.1**	**0.5**	**0.3**	**0.5**	**62**	**1**	**0.6**	100.0	**8**	**1%**
LOWER NIGER @ Itobe (sample 6234)																											
< 2	13%	class analyzed by XRD: **Kln**$_{59}$ **Sme**$_{2}$ **Ilt 40**												class not analyzed for heavy minerals													
2-5	2%	51	16	34	1.0	32%	0.5%	2.5	11	0	4	35	0.5	1.5	0.5	23	0	0.5	1	0.5	1	22	0	0	100.0	15	0%
5-15	4%	61	13	25	1.6	34%	0.5%	3.8	15	1	2	0.5	1	0.5	0	22	1	0.5	0.5	0	4	51	0.5	0	100.0	18	2%
15-32	10%	62	13	25	1.7	33%	1.6%	3.9	18	4	3	3	1	0.0	1	32	0	0	0.4	1	0	38	0.4	0	100.0	24	9%
32-40	4%	67	16	18	2.0	47%	0%	4.6	30	0.5	3	1	5	0.5	0	32	0.5	0	1	0	0	25	0.5	0.5	100.0	34	2%
40-63	18%	58	18	24	1.4	43%	0.1%	4.2	11	3	2	1	4	0.5	0	26	0.5	0.5	0.5	0.5	1	49	0.5	0.5	100.0	16	6%
63-80	13%	58	19	23	1.4	45%	0.2%	3	2	2	1	0.5	4	0.9	0	22	1	0	0	0	0.5	64	2	0	100.0	5	3%
80-125	21%	56	21	24	1.3	47%	0.2%	2	1	1	0.5	1	3	0.0	0	16	2	0	0	0	0.5	72	1	0.5	100.0	3	2%
125-180	6%	57	18	24	1.4	43%	0.3%	0.4	1	3	0.5	0	1	0.5	0.5	18	0.5	0	1	1	0	71	0.5	1	100.0	5	5%
180-250	2%	69	9	22	2.2	30%	0.9%	0.4	2	2	0	0	3	3	6	16	4	5	4	0.5	0	53	1	0	100.0	4	4%
250-355	1%	85	1	15	5.5	4%	1.2%	0.1	---	p	p	---	---	p	p	c	c	---	---	---	p	c	---	p		9	22%
355-500	1%	76	5	19	3	23%	1.3%	0.05	---	p	---	---	---	---	---	p	---	p	---	---	---	p	---	p		13	50%
500-1000	2%	89	1	11	8	6%	1.3%					class not analyzed for insufficient amount of heavy minerals															
1000-2000	1%	83	4	13	5	25%	0%					class not analyzed for insufficient amount of heavy minerals															
> 2000	1%	90	0	10	9	0%	0%					class not analyzed for insufficient amount of heavy minerals															
BULK	100%	**60**	**17**	**23**	**1.7**	**41%**	**0.5%**	**2.9**	**8**	**1**	**1**	**3**	**2**	**0.3**	**0.2**	**24**	**1**	**0.4**	**0.2**	**0.2**	**0.7**	**56**	**0.8**	0.02	100.0	**11**	**2%**

GSZ class	Class	MgO	CaO	TiO_2	MnO	Sr	Ba	Sc	Y	Th	Zr	Hf	La	Ce	Pr	Nd	Sm	Gd	Tb	Dy	Ho	Er	Yb	Lu	Zr/Hf	ε_{Nd}
	wt%	wt%	wt%	wt%	wt%	ppm	ppm	ppm	ppm	ppm	ppm	ppm	ppm	ppm	ppm	ppm	ppm	ppm	ppm	ppm	ppm	ppm				
µm	**MIDDLE NIGER** @ Jamata (sample S6232)																									
< 2	16%	0.9	0.0	0.9	0.0	33	252	19	24	22	96	3	46	93	11	40	8	5.8	0.9	5.0	0.9	2.5	2.4	0.3	35	-18.4
< 5	2%	1.2	0.5	1.3	0.0	78	474	20	38	24	379	10	62	131	15	55	11	8.0	1.3	7.4	1.4	3.8	3.9	0.6	37	-18.4
5-15	2%	0.8	0.9	1.0	0.0	141	704	12	49	22	1747	42	40	83	10	35	7	6.5	1.2	7.7	1.7	5.1	5.8	0.9	41	-15.9
15-32	6%	0.2	0.6	1.5	0.0	105	486	9	100	48	3148	126	89	185	21	78	15	13.1	2.3	15.6	3.5	10.2	12.1	1.9	25	-15.8
32-40	4%	0.2	0.9	1.5	0.0	154	682	8	77	50	3987	104	96	189	22	80	15	12.0	2.0	12.5	2.7	8.0	9.5	1.5	38	-17.3
40-63	17%	0.1	0.7	0.8	0.0	109	456	4	43	21	1737	38	46	93	10	38	7	6.0	1.0	6.6	1.5	4.4	5.1	0.8	46	-17.4
63-80	11%	0.2	1.0	0.7	0.0	148	601	3	24	16	1069	25	32	65	7	27	6	4.5	0.7	4.1	0.8	2.2	2.3	0.4	44	-16.7
80-125	15%	0.1	0.9	0.5	0.0	146	608	2	21	8	606	13	12	25	3	11	2	2.0	0.4	2.7	0.6	2.0	2.4	0.4	48	-14.9
125-180	8%	0.0	0.7	0.2	0.0	108	456	1	5	2	84	2	5	10	1	4	1	0.7	0.1	0.8	0.2	0.6	0.6	0.1	46	-15.1
180-250	4%	0.0	0.5	0.1	0.0	74	292	1	2	1	78	1	4	8	1	3	1	0.4	0.1	0.4	0.1	0.2	0.2	0.0	58	-15.1
250-355	3%	0.0	0.5	0.1	0.0	73	291	1	5	11	73	2	17	36	4	16	4	2.9	0.4	1.4	0.2	0.4	0.4	0.1	47	-18.3
355-500	3%	0.0	0.4	0.0	0.0	44	192	0	2	1	58	1	2	5	1	2	0	0.3	0.0	0.3	0.1	0.2	0.2	0.0	45	-20.1
500-1000	5%	0.0	0.4	0.0	0.0	36	118	0	2	2	64	1	4	8	1	3	1	0.4	0.1	0.4	0.1	0.2	0.2	0.0	52	-22.0
1000-2000	3%	0.0	0.5	0.1	0.0	93	291	1	3	3	136	3	28	51	3	8	1	0.6	0.1	0.6	0.1	0.3	0.3	0.0	49	-17.4
BULK		0.3	0.8	0.6	0.0	121	520	5	24	17	1018	23	33	67	8	29	5	4.2	0.7	4.1	0.8	2.4	2.7	0.4	44	-16.9
	BENUE RIVER @ Mozum (sample S6233)																									
< 2	14%	1.3	0.1	1.2	0.0	60	270	20	43	30	139	4	111	242	25	94	16	11.9	1.7	8.8	1.6	4.2	3.5	0.5	37	-11.6
< 5	2%	1.7	0.7	1.6	0.0	130	550	21	43	29	312	8	101	224	24	85	15	10.6	1.6	8.6	1.6	4.1	3.7	0.5	39	-11.8
5-15	1%	1.1	1.3	1.6	0.1	220	797	15	54	28	3377	84	62	131	14	52	10	8.1	1.4	8.8	1.9	5.7	7.1	1.1	40	-13.3
15-32	7%	0.5	1.8	1.8	0.1	349	1367	14	88	58	4785	169	96	191	22	81	15	12.2	2.1	13.6	3.0	9.2	11.7	1.9	28	-15.3
32-40	3%	0.4	1.4	1.2	0.0	300	1188	9	46	31	3690	120	51	105	12	45	9	6.6	1.1	6.9	1.5	4.9	6.7	1.1	31	-15.1
40-63	15%	0.4	1.6	1.2	0.0	333	1308	7	35	36	4421	96	64	126	14	51	10	6.8	1.0	6.0	1.2	3.7	4.7	0.8	46	-16.8
63-80	12%	0.3	1.5	0.9	0.0	306	1177	5	29	17	2233	50	34	71	8	31	6	4.7	0.8	4.7	1.0	3.0	3.6	0.6	45	-13.3
80-125	23%	0.3	1.4	0.5	0.0	326	1255	3	11	10	633	13	25	46	5	20	4	2.7	0.4	2.1	0.4	1.1	1.2	0.2	47	-12.9
125-180	13%	0.1	1.1	0.2	0.0	285	1141	2	4	2	265	6	8	15	2	6	1	0.8	0.1	0.8	0.2	0.4	0.6	0.1	42	-11.7
180-250	5%	0.1	0.9	0.2	0.0	201	880	1	4	2	88	2	8	18	2	7	1	1.0	0.1	0.8	0.1	0.4	0.4	0.1	45	-11.9
250-355	2%	0.0	0.7	0.1	0.0	152	664	1	3	2	100	2	6	14	1	5	1	0.7	0.1	0.6	0.1	0.3	0.3	0.0	51	-12.8
355-500	1%	0.0	0.7	0.0	0.0	135	653	1	4	2	72	2	6	16	1	5	1	0.7	0.1	0.6	0.1	0.4	0.4	0.1	44	-13.8
500-1000	1%	0.1	0.6	0.0	0.0	97	617	1	6	5	141	3	11	23	3	9	2	1.4	0.2	1.1	0.2	0.6	0.6	0.1	47	-21.4
1000-2000	1%	0.2	1.3	0.3	0.0	267	1522	3	10	6	359	8	20	42	4	16	3	2.2	0.3	1.9	0.4	1.0	1.1	0.2	45	-15.8
BULK		0.6	1.3	0.7	0.0	299	1163	7	23	16	1291	30	34	69	8	28	5	3.8	0.6	3.9	0.8	2.3	2.6	0.4	43	-12.7
	LOWER NIGER @ Itobe (sample S6234)																									
< 2	13%	1.2	0.1	1.3	0.1	56	247	20	28	30	134	4	72	154	17	60	11	7.8	1.1	6.1	1.1	3.0	2.7	0.4	37	-11.7
< 5	2%	1.3	0.6	1.5	0.0	122	540	18	32	29	358	9	72	159	17	60	11	7.5	1.2	6.6	1.2	3.3	3.1	0.5	40	-12.1
5-15	4%	1.1	0.9	1.7	0.0	185	771	16	51	35	2147	51	73	156	17	62	12	9.1	1.5	9.2	1.9	5.4	5.9	0.9	42	-12.9
15-32	10%	0.5	1.3	1.6	0.1	277	1120	11	67	43	4258	120	74	151	17	63	12	9.5	1.6	10.6	2.3	7.1	8.8	1.4	35	-15.0
32-40	4%	0.3	1.6	1.7	0.1	326	1265	11	89	59	5878	219	98	196	23	81	15	11.9	2.0	13.2	3.0	9.5	12.4	2.0	27	-16.4
40-63	18%	0.3	1.4	1.1	0.0	291	1134	6	39	37	4208	81	59	117	13	49	9	6.9	1.1	6.5	1.3	4.0	4.9	0.8	52	-17.4
63-80	13%	0.3	1.6	0.9	0.0	327	1236	5	24	22	1768	39	31	61	7	26	5	4.0	0.6	3.9	0.8	2.4	2.8	0.5	45	-15.6
80-125	21%	0.2	1.2	0.4	0.0	279	1100	2	16	8	516	12	18	33	4	14	3	2.3	0.4	2.5	0.5	1.6	1.7	0.3	42	-15.7
125-180	6%	0.1	0.9	0.2	0.0	206	933	1	16	5	205	4	10	20	2	8	2	1.8	0.4	2.5	0.5	1.6	1.6	0.2	47	-18.6
180-250	2%	0.0	0.4	0.1	0.0	76	366	1	52	7	33	1	3	7	1	3	1	3.3	0.9	7.2	1.7	5.1	4.5	0.6	37	-8.9
250-355	1%	0.0	0.6	0.0	0.0	74	399	1	12	3	67	2	7	13	1	5	1	1.2	0.3	1.9	0.4	1.2	1.2	0.2	42	-20.1
355-500	1%	0.0	0.5	0.1	0.0	64	334	1	9	3	208	4	6	11	1	5	1	1.0	0.2	1.5	0.3	0.9	1.0	0.1	52	-18.2
500-1000	2%	0.1	0.5	0.1	0.0	74	427	2	6	4	138	3	8	15	2	6	1	1.0	0.2	1.0	0.2	0.6	0.7	0.1	46	-21.0
1000-2000	1%	0.0	4.6	0.7	0.0	285	137	7	12	20	806	16	14	28	3	11	2	1.9	0.2	2.1	0.4	1.2	1.3	0.2	50	-14.9
BULK		0.4	1.4	1.1	0.0	297	1147	8	40	35	2925	68	66	135	16	57	11	8.0	1.2	7.1	1.4	4.0	5.0	0.8	43	-14.7

MINERALOGY	Middle Niger	Benue
X-RAY DIFFRACTION		
Clay mode (XRD)	0%	100%
Cohesive mud (XRD)	29%	71%
OPTICAL+ RAMAN		
fSi mode (L fraction)	32%	68%
fSi mode (H fraction)	29%	71%
fSi mode (L+H fractions)	30%	70%
cSi mode (L fraction)	5%	95%
cSi mode (H fraction)	28%	72%
cSi mode (L+H fractions)	12%	88%
VFS mode (L fraction)	0%	100%
VFS mode (H fraction)	7%	93%
VFS mode (L+H fractions)	0%	100%
CS mode (L fraction)	10%	90%
CS mode (L+H fractions)	16%	84%
Bulk sample (L fraction)	0%	100%
Bulk sample (H fraction)	22%	78%
Bulk sample (L+H fractions)	0%	100%
GEOCHEMISTRY		
Clay (elements)	32%	69%
Clay (Nd isotopes)	2%	98%
Clay (Hf isotopes)	14%	86%
Sand (elements)	18%	82%
Sand (Nd isotopes)	4%	96%
Sand (Hf isotopes)	19%	81%
Bulk sample (elements)	6%	94%
Bulk sample (Nd isotopes)	17%	83%
GEOCHRONOLOGY		
Zircon ages	12%	88%
GAUGED FLUXES		
Suspended load	29%	71%
Bedload	33%	67%
TOTAL		
Mean	**15%**	**85%**
standard deviation	*12%*	*12%*